OPEN ACCESS

Original research

Blockade of interleukin 10 potentiates antitumour immune function in human colorectal cancer liver metastases

Kevin M Sullivan ,[1] Xiuyun Jiang,[1] Prajna Guha,[2,3] Christopher Lausted,[4] Jason A Carter,[1] Cynthia Hsu,[1] Kevin P Labadie,[1] Karan Kohli,[1,5] Heidi L Kenerson,[1] Sara K Daniel,[1] Xiaowei Yan,[4] Changting Meng,[4] Arezou Abbasi,[1] Marina Chan,[6] Y David Seo,[1] James O Park,[1] Ian Nicholas Crispe,[7] Raymond S Yeung,[1] Teresa S Kim ,[1] Taranjit S Gujral ,[6] Qiang Tian,[4,8] Steven C Katz,[2,3] Venu G Pillarisetty [1,5]

► Additional supplemental material is published online only. To view, please visit the journal online (http://dx.doi.org/10.1136/gutjnl-2021-325808).

For numbered affiliations see end of article.

Correspondence to
Dr Venu G Pillarisetty, Surgery, University of Washington, Seattle, WA 98195, USA; vgp@uw.edu and Dr Qiang Tian, 197 Ruijin Er Road, Shanghai, People's Republic of China 200025; tq12221@rjh.com.cn

KMS and XJ contributed equally.

Received 5 August 2021
Accepted 25 May 2022
Published Online First 15 June 2022

To cite: Sullivan KM, Jiang X, Guha P, *et al*. *Gut* 2023;**72**:325–337.

ABSTRACT

Objective Programmed cell death protein 1 (PD-1) checkpoint inhibition and adoptive cellular therapy have had limited success in patients with microsatellite stable colorectal cancer liver metastases (CRLM). We sought to evaluate the effect of interleukin 10 (IL-10) blockade on endogenous T cell and chimeric antigen receptor T (CAR-T) cell antitumour function in CRLM slice cultures.

Design We created organotypic slice cultures from human CRLM (n=38 patients' tumours) and tested the antitumour effects of a neutralising antibody against IL-10 (αIL-10) both alone as treatment and in combination with exogenously administered carcinoembryonic antigen (CEA)-specific CAR-T cells. We evaluated slice cultures with single and multiplex immunohistochemistry, in situ hybridisation, single-cell RNA sequencing, reverse-phase protein arrays and time-lapse fluorescent microscopy.

Results αIL-10 generated a 1.8-fold increase in T cell-mediated carcinoma cell death in human CRLM slice cultures. αIL-10 significantly increased proportions of $CD8^+$ T cells without exhaustion transcription changes, and increased human leukocyte antigen - DR isotype (HLA-DR) expression of macrophages. The antitumour effects of αIL-10 were reversed by major histocompatibility complex class I or II (MHC-I or MHC-II) blockade, confirming the essential role of antigen presenting cells. Interrupting IL-10 signalling also rescued murine CAR-T cell proliferation and cytotoxicity from myeloid cell-mediated immunosuppression. In human CRLM slices, αIL-10 increased CEA-specific CAR-T cell activation and CAR-T cell-mediated cytotoxicity, with nearly 70% carcinoma cell apoptosis across multiple human tumours. Pretreatment with an IL-10 receptor blocking antibody also potentiated CAR-T function.

Conclusion Neutralising the effects of IL-10 in human CRLM has therapeutic potential as a stand-alone treatment and to augment the function of adoptively transferred CAR-T cells.

WHAT IS ALREADY KNOWN ON THIS TOPIC

⇒ Despite evidence that the immune system plays a role in tumour development and progression, immunotherapy has yet to demonstrate substantial benefit for patients with metastatic microsatellite stable (MSS) colorectal carcinoma. Although interleukin 10 (IL-10) is primarily believed to be an immunosuppressive cytokine, its role in advanced gastrointestinal malignancies remains unclear. A human tumour slice culture model serves as an accurate predictor of therapeutic drug effects on the tumour microenvironment (TME). In mouse models of colorectal cancer liver metastases (CRLM), myeloid cells are immunosuppressive and inhibit activity of anti-carcinoembryonic antigen chimeric antigen receptor T (CAR-T) cells.

WHAT THIS STUDY ADDS

⇒ IL-10 is produced by macrophages, T cells and tumour cells in CRLM. IL-10 blockade overcomes the immunosuppressive TME in a model of human CRLM and reactivates endogenous antitumour immunity, generating nearly twofold greater carcinoma cell death. IL-10 blockade dramatically enhances CAR-T cell cytotoxicity in vitro and in human CRLM slice cultures.

HOW THIS STUDY MIGHT AFFECT RESEARCH, PRACTICE OR POLICY

⇒ IL-10 represents a major immunosuppressive signal to overcome in patients with CRLM. Targeting IL-10/IL-10 receptor signalling has great potential to be incorporated into systemic therapy for patients with immune checkpoint blockade-resistant, MSS CRLM. CAR-T cells, armed against IL-10 suppression, may pave the way for more effective adoptive cell therapies for patients with MSS CRLM refractory to currently available surgical and medical therapies.

INTRODUCTION

Colorectal cancer (CRC) is the third most common cause of cancer-related mortality in the USA.[1] For the 25%–30% of patients with CRC who develop liver metastases, the 5-year overall survival (OS) rate is 49% with resection but only 2.2% with palliative chemotherapy. The profound impact of CRC liver

metastases (CRLM) is highlighted by the fact that the survival of CRC patients with isolated liver metastases is substantially worse than for those with isolated lung metastases.[2]

Immune checkpoint inhibition (ICI) with programmed cell death protein 1 (PD-1) blockade is effective in patients with microsatellite instability-high (MSI-H) CRC, but this represents less than 5% of patients with CRC with locally advanced or metastatic disease.[3] Among all patients with CRC, objective response rates to checkpoint blockade are seen in less than 5% of patients.[4–7] However, tumour-infiltrating lymphocytes correlate with prognosis. The Immunoscore, which grades $CD3^+$ and $CD8^+$ T cell density within CRLM, correlates with better prognosis,[8] and high regulatory T cell (Treg cell) infiltrate correlates with shorter OS.[9] Both the density and morphology of tumour-associated macrophages (TAMs) correlate with survival in patients with CRLM.[10 11] Despite the lack of success of currently approved immunotherapies, modulation of immune cells infiltrating CRLM remains a compelling potential therapeutic approach.

An alternative immunotherapeutic approach is adoptive transfer of chimeric antigen receptor T (CAR-T) cells, but several aspects of the CRLM tumour microenvironment (TME) limit the efficacy of CAR-T cells.[12] In a phase I clinical trial of anti-carcinoembryonic antigen (CEA) CAR-T cells for patients with CRLM who had progressed on other therapies, 7 of 10 patients demonstrated stable disease without severe adverse reactions.[13] A phase I trial of anti-CEA CAR-T administered via hepatic arterial infusion showed stable disease in one of six patients and tumour necrosis or fibrosis in four of six patients, without grade 3 or 4 adverse events.[14] In murine studies of the liver immune TME, myeloid cells suppress antitumour immunity via signal transducer and activator of transcription factor 3 (STAT3)-mediated expression of indoleamine 2,3-deoxygenase (IDO) and programmed death ligand 1 (PD-L1), and CAR-T efficacy can be rescued when murine myeloid cells are depleted.[15 16] The effect of the specific organ TME on the immune landscape in a tumour is evidenced by the finding that myeloid cells in liver metastases are more immunosuppressive than those isolated from lung metastases.[17] Importantly, the liver-specific myeloid cell functional programme was reversible on transfer into lung tissue, suggesting repolarisation of immunosuppressive liver TAMs as a novel therapeutic approach.

Interleukin 10 (IL-10) has broad immunosuppressive functions through interaction with its cognate receptor (IL-10R) and downstream activation of the STAT3 pathway. Classically, IL-10 inhibits antigen-presenting cells (APCs) leading to T cell inhibition, in addition to directly causing $CD4^+$ T cell anergy.[18] A variety of immunosuppressive signals, including IL-10, support a bias towards immune tolerance in the liver, which permits immunological silence towards antigens present in food.[19] In non-haematological malignancies including CRC, high serum IL-10 correlates with more advanced stage, worse survival or higher recurrence rate.[20 21] In a murine breast cancer model, IL-10 from macrophages suppressed dendritic cell (DC) IL-12 secretion to abrogate $CD8^+$ T cell responses.[22] In a murine CRC model, intratumoral injections of a lentiviral vector encoding IL-10-silencing short hairpin RNA (shRNA) reduced tumour growth.[23] Conversely, some studies have suggested a beneficial effect of IL-10 including increased $CD8^+$ cell infiltration and increased interferon-gamma release in the TME.[24–30] However, clinical trials using pegylated IL-10 treatment have not shown a benefit in patients.[31 32] Recent definition of the active structure of the IL-10 ligand/receptor suggests new ways of targeting the IL-10/IL-10R axis in a cell type-specific manner.[33]

Tumour slice culture (TSC) permits the evaluation of immune cell function in the context of the native three-dimensional (3D) solid tumour structure and cell populations. Our laboratory has demonstrated that the TME remains intact and viable in human TSC for 1–2 weeks[34–36] and that antitumour immunity can be enhanced in immune-excluded solid tumours such as pancreatic adenocarcinoma.[37] Notably, in TSC, combined CXCR4/PD-1 inhibition improved migration of cytotoxic T cells toward carcinoma cells, an effect mirrored in patients' tumours on a clinical trial of these therapies.[38] Because the effect of IL-10 on antitumour immune function remains controversial, we leveraged the human TSC system to investigate the role of IL-10 in human CRLM. We confirmed the inhibitory effect of IL-10 and demonstrated that IL-10 blockade dramatically enhanced antitumour function of both endogenous and adoptively transferred T cells in a heterogeneous cohort of human CRLM tumours.

MATERIALS AND METHODS

Ethics statement

All investigations were performed according to the principles expressed in the Declaration of Helsinki. Samples for slice culture were procured from patients undergoing hepatic resection for CRLM who provided prior written-informed consent under a research protocol (no. 1852) approved by the University of Washington Institutional Review Board.

Patient and public involvement

Patients were involved in providing voluntary consent for use of their tumour specimens. Patients were not involved in the research design, conduct, reporting or dissemination plans.

The Cancer Genome Atlas (TCGA) analysis

IL10 RNA expression and disease-specific survival (DSS) data from TCGA Pan-Cancer cohort was exported using the UCSC Xena webtool.[39] Only colon adenocarcinoma (COAD) primary tumours were included for the survival analysis, and duplicate samples were excluded. Kaplan-Meier DSS curves with 68% CIs were generated using the Python lifelines (v0.26.0) package.

Tumour slice culture

Slice culture of freshly resected human CRLM tumours was performed as previously described.[35–37 40] Additional details and treatment antibody data are available in online supplemental table S1. Slice cultures were treated with 20 µg/mL of each treatment antibody.

In situ hybridisation (ISH) and multicolour immunohistochemistry (mIHC)

Detailed description of ISH and mIHC, reagents and antibodies used are available in online supplemental table S2. Slides were imaged with Leica SP8X confocal microscope (Leica Microsystems, Wetzlar, Germany). Areas of nuclear overlap on the images were analysed using IMARIS (Bitplane USA) and Flowjo (Beckton Dickinson).

Reverse phase protein array (RPPA)

Protein microarrays were printed and processed as described previously.[41 42] Slides were scanned using Licor Odyssey CLX Scanner (LiCOR). Total signal intensity was normalised to total beta-actin (Sigma, Catalogue No A1978) and quantified using Array-Pro analyzer software package (Media Cybernetics, Maryland, USA).

Terminal deoxynucleotidyl transferase dUTP nick end labelling (TUNEL)

The Click-iT Plus TUNEL Assay for In Situ Apoptosis Alexa Fluor 488 dye kit (C10617, ThermoFisher) was used according to manufacturer instructions. Slides were imaged using Leica SP8X confocal microscope. After background intensity subtraction, automatic counting of total nuclei and colocalisation was performed in IMARIS using the spots colocalisation function.

Immunohistochemistry (IHC)

Detailed description of IHC steps, reagents used and primary IHC antibodies are available in the online supplemental table S3. The transversely cut slides were imaged at 20x to visualise the entire thickness of the slice. Slides were digitally scanned to NanoZoomer Digital Pathology (Hamamatsu) image viewing software. Positive 3,3'-diaminobenzidine (DAB) cells with haematoxylin-stained nuclei were visually counted using Fiji ImageJ software over at least two high-powered fields (hpf) per slice in at least two different slices per treatment per individual patient tumour.

RNA sequencing

Slices were treated and RNA extracted using Qiagen RNeasy kit according to the manufacturer's protocol. RNA sequencing was performed using the Northwest Genomics Center core facility with Next Generation Sequencing after samples passed quality controls. Samples were provided as normalised cell counts to housekeeping genes. The data have been deposited and are publicly available.[43]

Single-cell RNA sequencing (scRNAseq)

ScRNAseq was carried out first by dissociating untreated slices from fresh tumour tissue. Next, slices treated with either control or IL-10 blocking antibody were dissociated. After removal of dead cells and single-cell suspension preparation, 10× droplet sequencing was performed. Details of each steps and the statistical analysis are available in the online supplemental materials. The scRNAseq data have been deposited and are also available.[43]

Mice, liver metastasis (LM) in vivo model and myeloid cell isolation

C57BL/6 male mice (6–8 weeks old) obtained from Jackson Laboratories were bred and maintained under pathogen-free conditions at Roger Williams Medical Center (RWMC) animal facility. All surgical procedures were approved by RWMC Institutional Animal Care and Use Committee protocol No. 19-2904. To generate LM, mice were anaesthetised and injected with 2.5×10^6 cells via spleen followed by splenectomy. Liver non-parenchymal cells were isolated from LM, 4 days post-tumour generation, as previously described.[15] Immunomagnetic beads against CD11b were used to purify bulk hepatic myeloid cells (Miltenyi Biotech). Further details are available in the online supplemental materials.

CAR-T generation, proliferation assay and cytotoxicity assay

Using a construct provided by Sorrento and TNK Therapeutics, CAR-T cells were generated from mouse splenocytes as described previously[44] and MC38CEA cells were used as target tumour cells. Myeloid cells were isolated from LM tumour-bearing mice livers. CAR-T cells were carboxyfluorescein diacetate succinimidyl ester (CFSE, Life Technologies) labelled as per the manufacturer's protocol. MC38CEA cells were plated at 2×10^4 cells/well in 96-well cell culture plate with myeloid cells and CAR-T cells in a 1:1:1 ratio as controls. Cells were treated with 100, 200 or 400 ng/mL of anti-IL-10 antibody (JES5-2A5, BioLegend). Supernatant was collected and analysed for lactate dehydrogenase as per manufacturer's protocol (Promega). Antibodies used for flow cytometry are available in online supplemental table S4. Cells were collected for analysis using Cytoflex LX (Beckman Coulter), and postacquisition analysis was performed using FlowJo software.

Live imaging

CAR-T cells were stained with CFSE. One million untransduced control or anti-CEA CAR-T cells were added to slices in culture with either IgG antibody control or anti-IL-10 antibody (IL-10) and incubated for 1 day before imaging. Alternatively, the CAR-T cells were thawed and incubated overnight with 20 µg/mL of either control or anti-IL-10R antibody (IL-10R). The pretreated CAR-T cells were then stained, placed directly into the CRLM tissue slice culture media without additional treatment and incubated for 1 day before imaging. Live fluorescent microscopy was performed as previously described on a Leica SP8X confocal microscope.[37 40] Image processing and data analysis were performed on Leica LAS X software and IMARIS software. All $EpCAM^+$, $CFSE^+$, SR-$FLICA^+$ cells were counted manually throughout the time imaged at each position.

Flow cytometry

CAR-T cells were stained with CFSE. TSC slices were then treated with control or antigen-specific CAR-T cells with or without IL-10, and following treatment for 1 day in culture the slices were digested to a cell suspension. The cells were then stained with fluorophore-labelled CD69 and CD25 (online supplemental table S4), and flow cytometry was performed. The flow analysis was performed on the LSR2 and Symphony flow cytometry machines (Beckton Dickinson).

Statistical analysis

Statistical significance in the TCGA analysis between the first and fourth *IL10* expression quartiles was calculated using the Xena webtool's implementation of the log-rank test. Data were entered and analysed using Prism (GraphPad, La Jolla, California, USA). For all other experiments, Student's t-test, paired t-test or one-way analysis of variance with multiple comparisons was used as indicated. Statistical significance was defined as $p<0.05$. Further details are available in the online supplemental materials.

RESULTS

Patient and tumour characteristics

We generated TSC from 38 individual patients with CRLM (table 1). Microsatellite instability testing was available in 31 cases, and tumours were found to be microsatellite stable (MSS) in all available cases. All tumours treated with anti-CEA CAR-T cells were procured from patients with serum CEA greater than 2 ng/mL.

IL-10 blockade induces carcinoma cell death in human CRLM slice cultures refractory to PD-1 blockade

Analysis of TCGA Pan-Cancer dataset showed that elevated *IL10* expression correlated with worse 5-year DSS in patients with COAD (online supplemental figure S1). In contrast, transcript levels of *PDCD1* and *HACVR2*, encoding the T-cell coinhibitory receptors PD-1 and T-cell immunoglobulin and mucin domain-3 (TIM-3), respectively, did not correlate with DSS (online

Table 1 Characteristics of patients and tumour samples studied (n=38)

Clinicopathological characteristics	
Age, median (range)	56.5 (38–74) years old
Female	19/38 (50%)
Received neoadjuvant chemotherapy prior to hepatic resection	31/38 (82.6%)
Rectosigmoid or rectal location of primary tumour	17/38 (45.7%)
T stage of primary tumour	
T1	2/38 (5.3%)
T2	5/38 (13.2%)
T3	23/38 (60.5%)
T4	8/38 (21.1%)
N stage of primary tumour	
N0	9/38 (23.7%)
N1	17/38 (44.7%)
N2	12/38 (31.5%)
Lymphovascular invasion present in primary tumour (unknown for n=11)	19/27 (70.4%)
Perineural invasion present in primary tumour (unknown for n=10)	10/28 (35.7%)
Synchronous metastasis (unknown for n=2)	23/36 (63.9%)
Tumour molecular characteristics	
MSS (unknown for n=7)	31/31 (100%)
NRAS wild type (unknown for n=12)	25/26 (96.2%)
KRAS wild type (unknown for n=8)	21/30 (70%)
BRAF wild type (unknown for n=12)	26/26 (100%)

MSS, microsatellite stable .

supplemental figure S1). To determine the cell types producing and responding to IL-10 in CRLM, we performed single-cell RNA sequencing (scRNAseq) of fresh, untreated CRLM samples from three separate patients. Immune cells, defined by clusters with high expression of *PTPRC* encoding CD45, comprised an average of 11.1% (range 4.2%–31.4% in the three cases) of all cells. This immune cell population is primarily composed of macrophages, with a cluster high in both *CD68* and *CD163* expression (5.5% of all cells, 56.7% of immune cells), and *CD3* expressing T cells (3.3% of all cells, 33.9% of immune cells) (figure 1A). Of the T cells found within the CRLM tumour, the majority were helper T cells (Th) or cytotoxic T cells, with a smaller proportion of Treg cells (figure 1B). B cells expressing *CD79A* and DCs combined made up less than 0.3% of all cells and 3.4% of immune cells (figure 1A).

Analysis of our scRNAseq dataset demonstrated that while detectable RNA expression of IL-10 was predominantly limited to the TAM cluster, there was less, but still detectable, expression of *IL10* in the Th cluster, the IL-10 receptor gene (*IL10RA*) was highly expressed in both T cells and TAMs (figure 1A,B). Given the relatively high expression necessary to reliably identify a transcript via scRNAseq, we next sought to confirm these results using a more sensitive multiplexed in situ hybridisation (mISH) platform. We examined *IL10* and *IL10RA* gene expression in CRLM sections concurrently stained for carcinoma cells (EpCAM), T cells (CD3) and macrophages (CD68/CD163) (n=6). This mISH confirmed expression of *IL10* in 30.9% of macrophages, in addition to relatively low levels of transcript expression in 25.6% of T cells and 19.3% of carcinoma cells (figure 1C). As with the single-cell data, via mISH *IL10RA* was robustly expressed in TAM (25.0%) and T cells (14.9%), with expression rarely detected in carcinoma cells (3.1%, figure 1C).

Leveraging our human TSC experimental system, we next aimed to examine the effects of IL-10 and PD-1 blockade in CRLM. Consistent with clinical trial results,[45] anti-PD-1 did not increase tumour apoptosis compared with control in four individual human CRLM slice cultures (figure 2A,B). Given the inverse correlation between *IL10* expression and DSS, we posited that intratumoral IL-10 suppresses effective antitumour immune responses. We first confirmed that addition of an IL-10 neutralising monoclonal antibody (αIL-10) significantly reduced IL-10 protein from 8.5 pg/mL to 0.39 pg/mL in supernatant from CRLM slice cultures (n=5, online supplemental figure S2A). In the majority of 32 unique CRLM patients' TSCs, αIL-10 caused dramatic tumour necrosis (figure 2A), leading to 1.8-fold increased apoptosis compared with control (median 51.3% vs 29.1% cleaved Caspase-3$^+$ cells, p<0.0001; figure 2C). Cleaved Caspase-3 colocalised with EpCAM, an epithelial marker, confirming that apoptosis occurred predominantly in carcinoma cells, which comprise the bulk of cells within CRLM (online supplemental figure S2B). We saw a similar magnitude of αIL-10-induced tumour apoptosis when evaluating αIL-10 versus control-treated tumour slices for cleaved Caspase-3 protein expression via RPPA (mean relative signal intensity 2.1 vs 1.1 a.u., n=3 cases, p=0.015; figure 2D) and TUNEL (median 38.8% vs 20.3% TUNEL$^+$ of total nuclei, n=4 cases, p<0.001; figure 2E). Together, these results demonstrate the ability of IL-10 blockade to induce tumour-specific apoptosis in a human CRLM TSC model.

IL-10 blockade-mediated cell death in human CRLM is a result of immune activation

Given the ability of IL-10 blockade to specifically increase tumour cell death in our human CRLM TSC model, we hypothesised that IL-10 blockade in CRLM promotes a shift towards an inflammatory antitumour immune response in the TME. To further explore this hypothesis, we first quantified the presence of immune cells within each TSC treated with control antibody or IL-10 blockade. We found that the frequency of CD163$^+$ macrophages was not significantly different (p=0.17) between control and αIL-10 treated tumours (figure 3A), but there was an increase in the number of HLA-DR$^+$ cells (median 19.5% vs 11.5%, n=5 cases, p=0.02; figure 3B).

While αIL-10 did not alter the CD4$^+$ cell frequency (figure 3C), αIL-10 doubled the frequency of intratumoral CD8$^+$ cells compared with control (median 17.8% vs 7.0%, n=5, p=0.02; figure 3D). Similarly, αIL-10 increased gene expression of the immunostimulatory cytokine interferon-gamma, *IFNG*, when normalised to total cell number on days 2–5 (median 2.9% vs 2.3%, respectively, p<0.05, n=6; figure 3E) and a non-statistically significant increase in total granzyme B (mean 2.3% granzyme B positive tissue area vs 1.2%, n=6, p=0.13; online supplemental figure S2D). Although PD-1 does serve as a marker of T-cell exhaustion following prolonged (greater than 1 week) antigen stimulation,[46] we tested its expression after 2–5 days in our TSC model to identify early activated T cells potentially undergoing clonal expansion.[47 48] We found a non-statistically significant increase in CD3$^+$ T-cell expression of PD-1 in αIL-10-treated slices (p=0.08; online supplemental figure S2D), suggesting a shift towards an activated or clonally expanding phenotype.

To further understand the effects of IL-10 blockade on the immune TME, we additionally performed scRNAseq of αIL-10- and control-treated human CRLM TSCs from two individual patients at three consecutive time points (days 1, 2 and 3). We

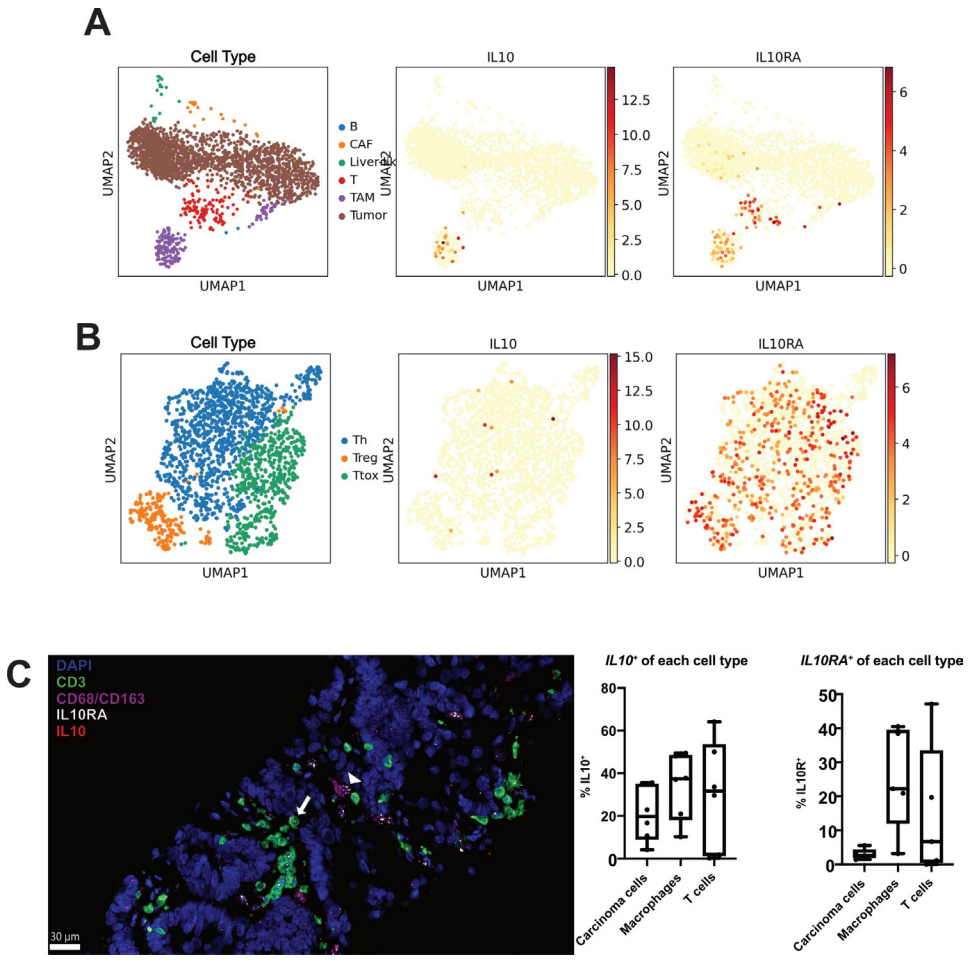

Figure 1 Interleukin 10 (IL-10) is produced by carcinoma cells, macrophages and T cells. (A) UMAP plots of all cell clusters of single cell RNA sequencing (scRNAseq) data from n=3 colorectal cancer liver metastases (CRLM) tumours. TAM, tumour-associated macrophages (purple); CAF, cancer-associated fibroblasts (orange); B cells (blue); liver-like cells (green); T cells (red); tumour cells (brown). *IL10* and *IL10RA* expression highlighted in red/orange. (B) UMAP plots of T cell cluster of scRNAseq data from n=3 CRCLM tumours. Th, helper T cells (blue); Ttox, cytotoxic T cells (green); Treg, regulatory T cells (orange). *IL10* and *IL10RA* expression highlighted in red/orange. (C) Multiplex immunohistochemistry was performed for T cells (CD3, green), macrophages (CD68/CD163, pink) and nuclei (DAPI, blue) with additional in situ hybridisation for *IL10* (red) and *IL10RA* (white). A representative image with *IL10*$^+$ *IL10RA*$^+$macrophage (white arrowhead) and *IL10*$^+$ *IL10RA*$^+$T cell (white arrow) is shown. Quantification of the proportion of *IL10*$^+$ and *IL10*$^+$ cells within each cell type is also shown (n=5 patient tumours). Scale bar=30 µm. Data points represent each human tumour sample.

captured a total of approximately 7300 cells across a total of six biological replicates. While not significant, we found that activation signature (*CD69*, *FASLG*, *CD27*, *CD28*, *TNFRSF9*, *TNFRSF4*, *LAMP1*, *EOMES*, *TBX21*) scores for both CD4$^+$ and CD8$^+$ T cells were higher in αIL-10-treated samples when compared with controls at each of the three examined time points (online supplemental figure S3A,B). Importantly, no such trend was observed for a T cell exhaustion signature (*PDCD1*, *CTLA4*, *HAVCR2*, *TIGIT*, *LAG3*) across treated and untreated samples (online supplemental figure S3C). We additionally observed a non-significant upregulation in MHC-II presentation Reactome pathway genes in TAMs (online supplemental figure S3D), which closely mirrored our previous IHC findings (figure 3A,B). As HLA-DR and CD163 colocalised on sequential IHC staining (n=4; online supplemental figure S2C), these results together strongly suggest that IL-10 blockade increases macrophage MHC-II expression and thereby macrophage activation. These findings thereby suggest that the antitumour immune response induced by IL-10 blockade is mediated by an increase in the frequency of CD8$^+$ cytotoxic T cell and concurrent immunostimulatory polarisation of TAMs.

We next sought to confirm the role of both direct CD8$^+$ cytotoxic T cell activity and indirect CD4$^+$ helper T cell and TAM activity in the αIL-10 antitumour response. Towards this, we treated CRLM tumours with αIL-10 in the presence or absence of antibody-mediated MHC class I or class II blockade. Confirming our hypothesis, we found that blockade of MHC-I, required for cytotoxic T cell antigen recognition, reversed the effects of IL-10 blockade on carcinoma cell apoptosis. In addition, blockade of MHC-II, required for CD4$^+$ T cell and TAM antigen presentation, similarly completely and independently abrogated the effects of αIL-10 (figure 3G). That is, these results directly demonstrate that both the MHC-I and MHC-II pathways are necessary, though not necessarily sufficient, for the IL-10 blockade-mediated antitumour immune response. In sum, our results demonstrate that IL-10 blockade in human CRLM TSC induces and requires a classical antitumour immune response involving the activation of cytotoxic T cells and APCs.

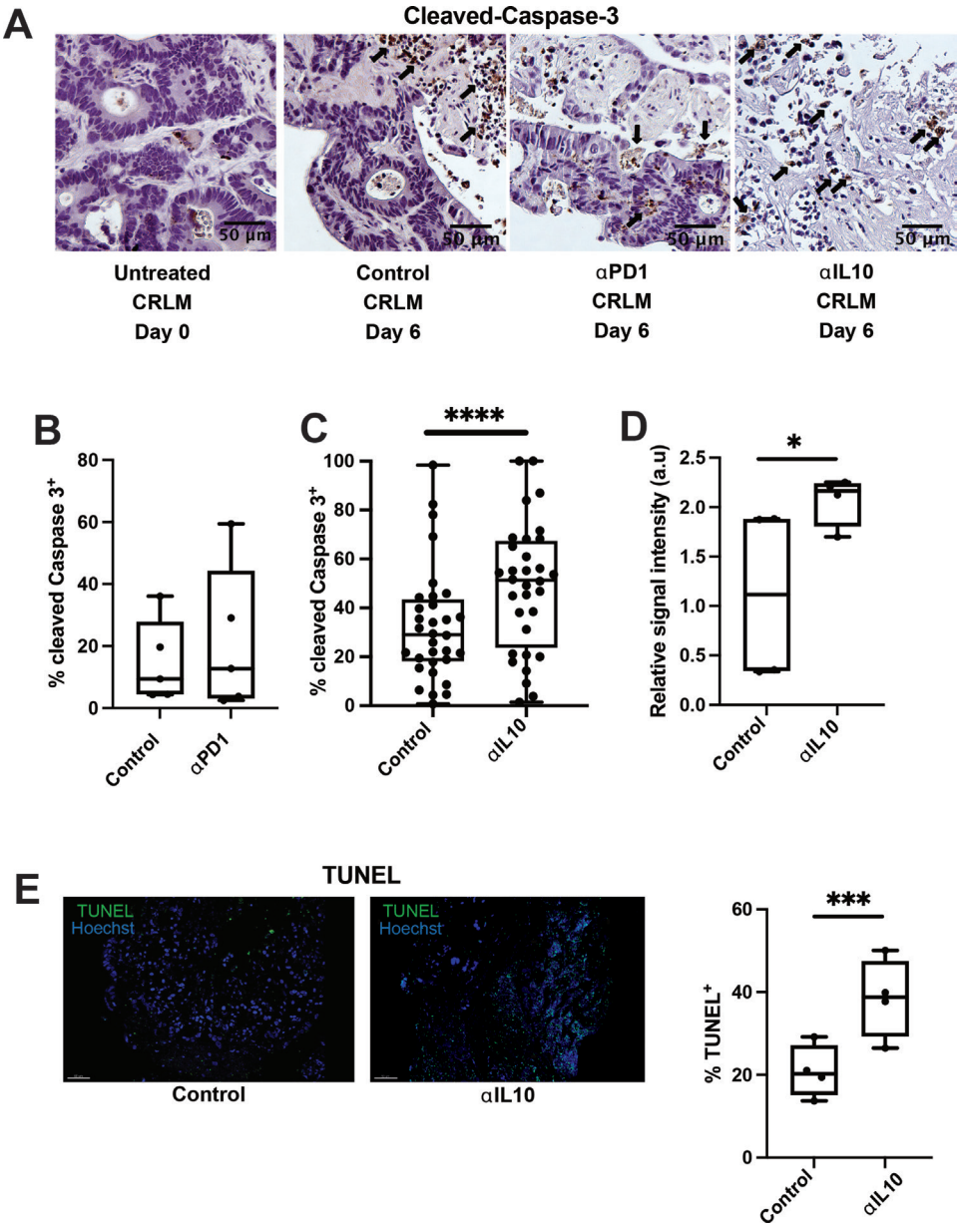

Figure 2 Interleukin 10 (IL-10) blockade facilitates significantly increased apoptosis of carcinoma cells. (A) Immunohistochemistry (IHC) for cleaved Caspase-3 was performed on tumour slice culture (TSC) after 6 days of treatment with immunomodulating agents. Representative images at 20x magnification from day 0, and then day 6 of antibody control, anti-programmed cell death protein-1 (anti-PD-1) antibody and αIL-10 treated slices. Black arrows denote apoptotic cells positive for cleaved Caspase-3 (brown). Scale bar=50 µm. (B) Quantification of percentage of cleaved Caspase-3$^+$ cells in slices treated with control or anti-PD-1 antibody (n=4 separate human cases with at least two slices per case). (C) Quantification of percentage of cleaved Caspase-3$^+$ cells in slices treated with control or αIL-10 (n=32 separate human cases with at least two slices per case). Data points represent each human tumour sample which consists of counts over multiple high-powered fields (hpf) in multiple slices to account for intratumoral heterogeneity. Student's t-test. ****p<0.0001. (D) Reverse phase protein array with relative signal intensity of total cleaved Caspase-3 in colorectal cancer liver metastases TSC after 6 days in culture with αIL-10 (n=4 cases). Student's t-test. *p<0.05. (E) Terminal deoxynucleotidyl transferase dUTP nick end labeling (TUNEL) staining with fluorescent microscopy demonstrating TUNEL$^+$ cells (green) after 6 days of αIL-10 (n=4 separate human cases). Scale bar=30 µm. Data points represent each human tumour sample which consists of counts over multiple hpf in multiple slices to account for intratumoral heterogeneity. Student's t-test. ***p<0.001.

Murine myeloid cell-derived IL-10 reversibly suppresses CAR-T cell proliferation

We previously demonstrated in a murine model of CRLM that myeloid cells suppress inflammation and inhibit CAR-T cell function in a STAT-3-dependent manner.[15 16] Based on our present findings on the effect of αIL-10 on native immune cells in the CRLM TME, we hypothesised that tumour-associated myeloid cells were suppressing CAR-T cells by secreting IL-10 and causing downstream IL-10R/STAT3 signalling in adjacent CAR-T cells. By flow cytometry, we found 37.4% of murine myeloid cells expressed IL-10, while few T cells produced IL-10 (figure 4A). In addition, multiplexed immunofluorescent imaging confirmed the presence of IL-10$^+$CD11b$^+$GR1$^+$ myeloid-derived suppressor cells and IL-10RA$^+$CD3$^+$ T cells (figure 4B). Addition of myeloid cells to coculture of anti-CEA CAR-T cells and CEA-expressing carcinoma cells significantly reduced CAR-T

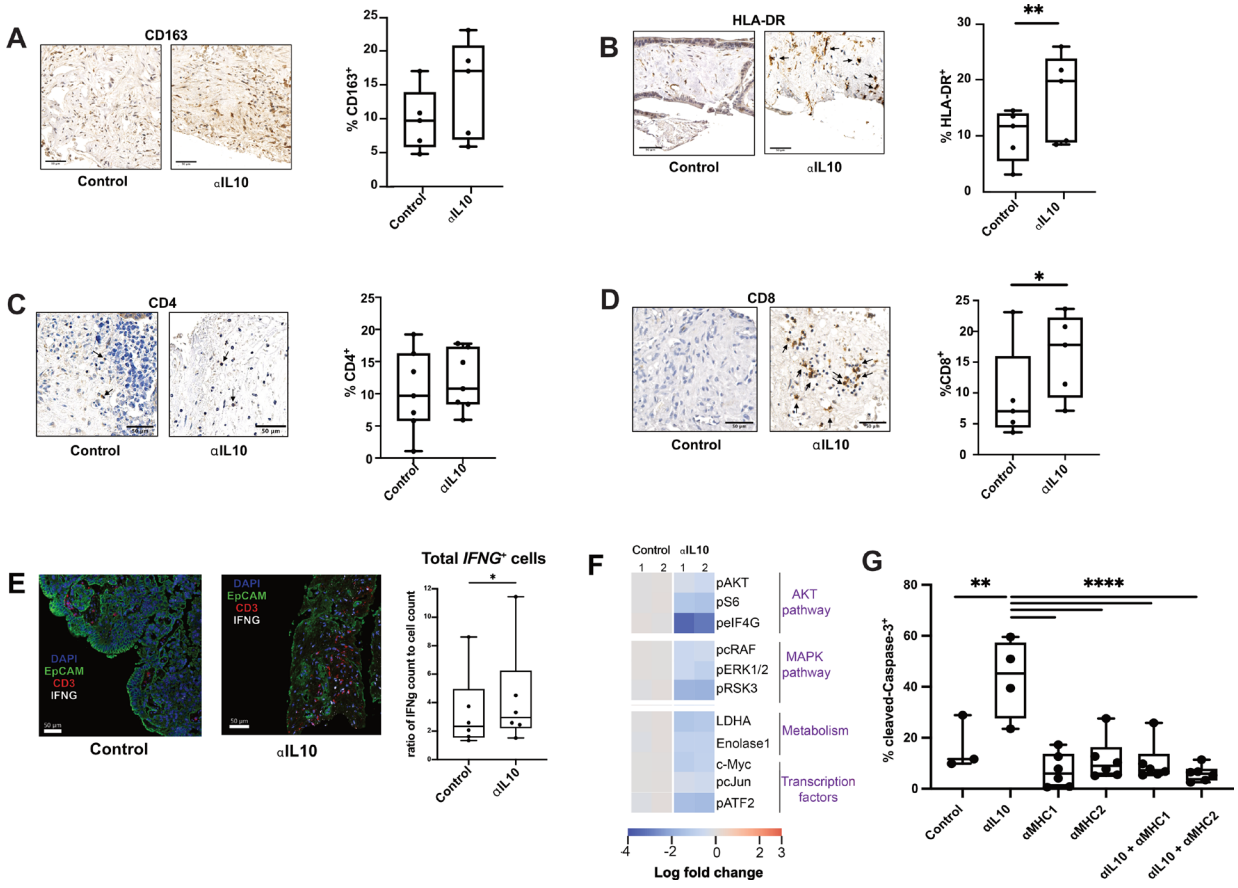

Figure 3 Increased CD8$^+$ T-cell population and inflammatory immune microenvironment occurs after interleukin 10 (IL-10) blockade. (A) Representative images at 20x magnification from IHC staining for CD163 of fixed TSC treated with control or αIL-10 after 4 days and quantification by cell count of CD163$^+$ cells (n=5 separate human tumours). Scale bar=50 µm. Data points represent each human tumour sample which consists of counts over multiple hpf in multiple slices to account for intratumoral heterogeneity. Not significant by Student's t-test. (B) Representative images at 20x magnification from IHC of fixed TSC treated with control or αIL-10 after 4 days, with black arrows denoting HLA-DR$^+$ cells, and quantification by cell count of HLA-DR$^+$ cells (n=5 separate human tumours). Scale bar=50 µm. Data points represent each human tumour sample which consists of counts over multiple hpf in multiple slices to account for intratumoral heterogeneity. Student's t-test. *p<0.05. (C) Representative images at 20x magnification from IHC of fixed TSC treated with control or αIL-10 after 4 days, with black arrows denoting CD4$^+$ cells, and quantification by cell count of CD4$^+$ cells (n=7 separate human tumours). Scale bar=50 µm. Data points represent each human tumour sample which consists of counts over multiple hpf in multiple slices to account for intratumoral heterogeneity. (D) Representative images at 20x magnification from IHC of fixed TSC treated with control or αIL-10 after 4 days, with black arrows denoting CD8$^+$ cells. Quantification by cell count of CD8$^+$ cells (n=5 separate human tumours). Scale bar=50 µm. Data points represent each human tumour sample which consists of counts over multiple hpf in multiple slices to account for intratumoral heterogeneity. Student's t-test. *p<0.05. (E) Multiplex IHC was performed for T cells (CD3, red), carcinoma cells (EpCAM, green) and nuclei (DAPI, blue) with additional in situ hybridisation for *IFNG* (white). Quantification of proportion of *IFNG*$^+$ per total number of cells by ISH and by IHC are also shown (n=6 patient tumours). Scale bar=50 µm. Data points represent each human tumour sample. Student's t-test. *p<0.05. (F) RPPA data from slices treated with antibody control or IL-10 blockade showing downregulation of various molecular pathways. (G) Quantification of percentage of cleaved Caspase-3$^+$ cells following αIL-10 with or without MHC blockade shows that while αIL-10 alone increases apoptotic cell proportion, the effect is reversible with MHC blockade back to below baseline levels of cell death. Representative data with data points representing a slice from one human tumour experiment, repeated in a total of three human tumour samples with similar results. Error bars display SEM. ANOVA with multiple comparisons. **p<0.01, ****p<0.0001.

cell proliferation from 50.3% to 29.3% (figure 4C). However, when the CAR-T cell, carcinoma cell and myeloid cell cocultures were treated with αIL-10, CAR-T proliferation was restored in a dose-dependent fashion (39.7%–45.9% proliferation, n=4, p<0.01; figure 4C). Myeloid cells also possess the ability to inhibit the cytotoxic activity of CAR-T cells. Importantly, as with its effect on CAR-T proliferation, addition of αIL-10 to the coculture system reversed the suppressive effects of myeloid cells on tumour cytotoxicity (p<0.001; figure 4D). Therefore, our results demonstrate that myeloid cell suppression of anti-CEA CAR-T cell proliferation and cytotoxicity can be reversed by antibody neutralisation of IL-10.

IL-10 blockade facilitates CAR-T-mediated tumour cell death

Based on our results in murine CRLM, we hypothesised that αIL-10 would also enhance cytotoxicity of CEA-specific CAR-T cells in human CRLM. We previously demonstrated the ability of intravital confocal microscopy to demonstrate early effects of T cell-targeted therapies in human PDA slice cultures.[37] We first confirmed adequate migration of CAR-T cells into the tumour slice after 1 day (figure 5A). We then used live imaging to assess CAR-T function in the presence of αIL-10 or control. CEA-specific CAR-T cells demonstrated low (mean 30.1%) basal migration to target cells (defined by EpCAM$^+$ cell with CFSE$^+$

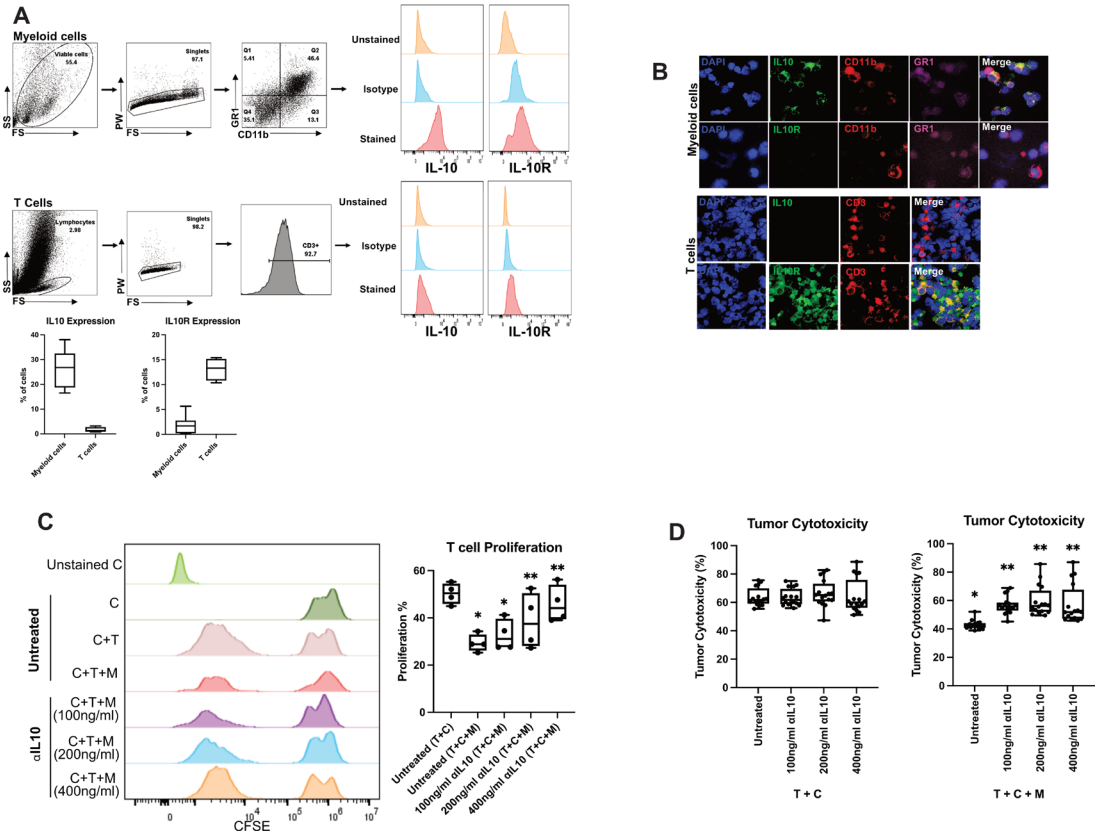

Figure 4 Treatment with interleukin 10 (IL-10) antibody reverses murine myeloid cell suppressive activity of chimeric antigen receptor T (CAR-T) cells. (A) Phenotypic characterisation of CAR-T cells and CD11b$^+$ cells isolated 4 days post-tumour generation was performed as per the gating strategy. Representative flow cytometry plots showing expression of IL-10 and IL-10R for myeloid cells (n=7) and CAR-T (n=4). (B) Immunofluorescence performed on CAR-T and myeloid cells confirmed expression of IL-10 (green) in myeloid cells and IL-10R (green) on CAR-T cells. (C) Carboxyfluorescein diacetate succinimidyl ester (CFSE)-labelled CAR-T (C) cells were cocultured with myeloid cells (M) isolated from liver metastases (LM) tumour-bearing mice and MC38CEA tumour cells (T) in 1:1:1 ratio. Cells were treated with 100 ng/mL or 200 ng/mL or 400 ng/mL anti-IL-10 antibody for 24 hours. *p<0.005 versus untreated (T+C), **p<0.01 versus untreated (T+C+M). (D) The in vitro cytotoxic activity of CAR-T (C) cells was evaluated by incubating MC38CEA (T) cells with myeloid cells (M) treated with at a 1:1:1 ratio as shown in C. Corresponding tumour and CAR-T controls were used for the assay. *p<0.0001 versus T+C, **p<0.001 versus untreated T+C+M. All data were analysed by one-way analysis of variance and Tukey's test or two-sided Student's t-test.

CAR-T cell within 20 µm), which was enhanced with addition of αIL-10 (mean 82.5%, n=3 separate CRLM tumours, p<0.001; figure 5B). Additionally, there was lower antitumour activity in the control or antigen-specific CAR-T cells treated with control when compared with αIL-10 (67.2% vs 15.6%–26.6% SR-FLICA$^+$ EpCAM$^+$ cells, n=3 cases, p<0.03; figure 5C). To determine if the increase in cancer cell death was mediated by CAR-T cells and not another cell type, we specifically evaluated the subset of carcinoma cells adjacent to a CAR-T cell. We found 58.2% of EpCAM$^+$ cells adjacent to anti-CEA CAR-T cells were SR-FLICA$^+$ when treated additionally with αIL-10, while this was true of only 18.7% of EpCAM$^+$ cells treated with anti-CEA CAR-T cells in the absence αIL-10 (p=0.007, n=3 separate human CRLM tumours; figure 5D). Additionally, there was no difference in the proportion of SR-FLICA$^+$ EpCAM$^+$ cells not adjacent to a CFSE$^+$ CAR-T cell. Together, these results demonstrate that IL-10 inhibits tumour-specific CAR-T function in both human and murine CRLM.

To better characterise the downstream effects of IL-10 blockade on antigen-specific CAR-T cells in human CRLM, we performed RNA sequencing of the treated human tumour slices after 1 day. We specifically found that genes associated with cytolytic functions (*GNLY*, *GZMA*, *PRF1*), inflammation (*IFNG*, *GBP5*,[49] *NOS2*) and T cell migration/chemotaxis (*CXCL9*, *CXCL10*, *CXCL11*,[50] *CCL7*, *CCL8*) were relatively upregulated after antigen-specific CAR-T cells were treated with αIL-10 (figure 6A). We then performed a gene ontology analysis of upregulated genes in those samples treated with anti-CEA CAR-T cells and αIL-10 versus anti-CEA CAR-T cells and control IgG. Transcriptional pathways including cellular response to interferon-gamma, inflammatory response, cellular response to IL-1, lymphocyte chemotaxis and T cell migration were all upregulated in the antigen-specific CAR-T cells treated with αIL-10 compared with the same CAR-T cells treated with control antibody (figure 6B). Additionally, flow cytometry performed on the CAR-T cells after coculture in slice culture demonstrated increased expression of the activation markers CD25 and CD69 (figure 6C; online supplemental figure S5).

To determine the molecular mechanisms within the CAR-T cells, we employed RPPA to assess changes in the state and activity of >20 proteins including major oncogenic signalling pathways (RAF/MEK/ERK, PI3K/AKT, RTK signalling and STATs) in slices treated with anti-CEA CAR-T cells and αIL-10. We found a decrease in pS6 ribosomal protein expression within 24 hours followed by a decrease in STAT1 at 48 hours (figure 6D). Cleaved Caspase-7 increased in the anti-CEA CAR-T and αIL-10-treated

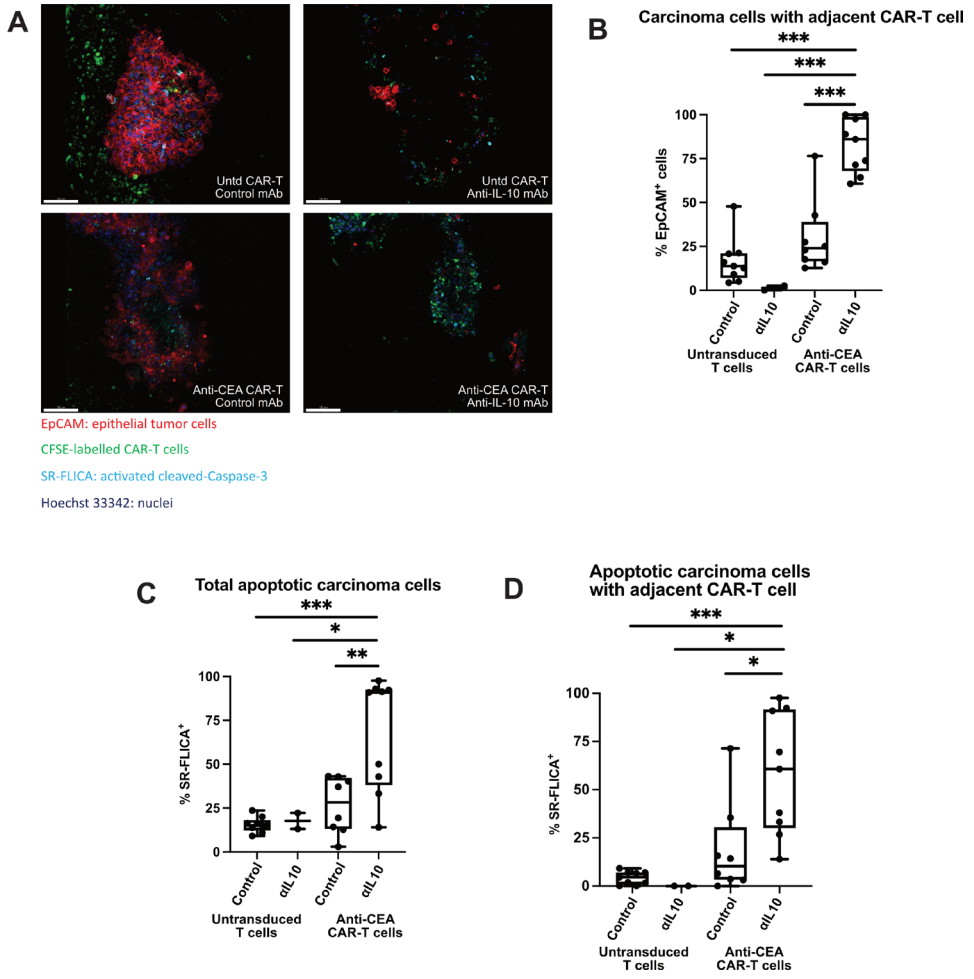

Figure 5 Interleukin 10 (IL-10) blockade enhances chimeric antigen receptor T (CAR-T) cell migration and tumour apoptosis. (A) Live staining and fluorescent microscopy of colorectal cancer liver metastases (CRLM) tumour slice culture (TSC) treated with untransduced CAR-T with control, untransduced CAR-T with αIL-10, anti-carcinoembryonic antigen (CEA) CAR-T with control, and anti-CEA CAR-T with αIL-10 show CFSE$^+$ CAR-T cells (green) within the tumour and near epithelial carcinoma cells (red) when antigen-specific CAR-T are used in combination with αIL-10. Apoptotic cells are shown when activated cleaved Caspases are present and positive for the SR-FLICA reagent (cyan). Tumour slices were imaged after 1 day of treatment. Scale bar=100 µm. (B) Quantification of the carcinoma cells with a CAR-T cell nearby (defined as within 20 µm) with untransduced control CAR-T cells and anti-CEA CAR-T cells treated concurrently with or without αIL-10. Data points represent each high-powered fields (hpf) area imaged, with 3 hpf imaged in each tumour (n=3 separate human tumour samples). Analysis of variance with multiple comparisons. ***p<0.001. (C,D) Quantification of the percentage of total carcinoma cells that are SR-FLICA$^+$, and SR-FLICA$^+$ carcinoma cells with a CAR-T cell nearby (defined as within 20 µm) after untransduced control CAR-T and anti-CEA CAR-T cells are treated concurrently with or without αIL-10. Data points represent each hpf area imaged, with 3 hpf imaged in each tumour (n=3 separate human tumour samples). Analysis of variance with multiple comparisons. *p<0.05, **p<0.01, ***p<0.001.

slices in 6 hours and was then low at 48 hours. At 48 hours, we noted an increase in nuclear factor kappa B (NF-κB) expression. NF-κB is unlikely to be upregulated in dying tumour cells and therefore this change likely represents CAR-T cells as the next most abundant cell type, and high NF-κB activity has been demonstrated in antitumour T-cell responses.[51–53] The time course of the increase in cleaved Caspase is consistent with our findings of increased cell death in about within 1 day as previously described on fluorescence imaging, and the subsequent decrease may be due to early significant cell death leading to less Caspase activity at later time points. In addition, we noted high NF-κB activity after 24–48 hours, consistent with our findings of increased antitumour activity of the antigen-specific CAR-T cells within 2 days.

Given the rapid effect of αIL-10 on CAR-T function, we hypothesised that this was due to relief of direct suppressive effects of IL-10 on CAR-T cells, rather than from secondary effects attributable to modulation of myeloid cells. To test this hypothesis, we pretreated the CAR-T cells with an antagonistic anti-IL-10 receptor alpha (IL-10R) antibody before adding them alone to the CRLM TSC. CAR-T cells pretreated with αIL-10R showed a trend towards being in closer proximity to carcinoma cells compared with control treated CAR-T (figure 6E). Furthermore, pretreatment with αIL-10R increased CAR-T cytotoxicity, as evidenced by increased total carcinoma cell apoptosis, and apoptosis with an adjacent CAR-T cell (p<0.05; figure 6F,G). These data demonstrate that IL-10 blockade activates CAR-T cell function in part through direct inhibition of IL-10R signalling in CAR-T cells.

DISCUSSION

Defining tumour-specific mechanisms of immune evasion is critical to developing new immunotherapies against ICI-resistant cancers, and testing these strategies in accurate preclinical

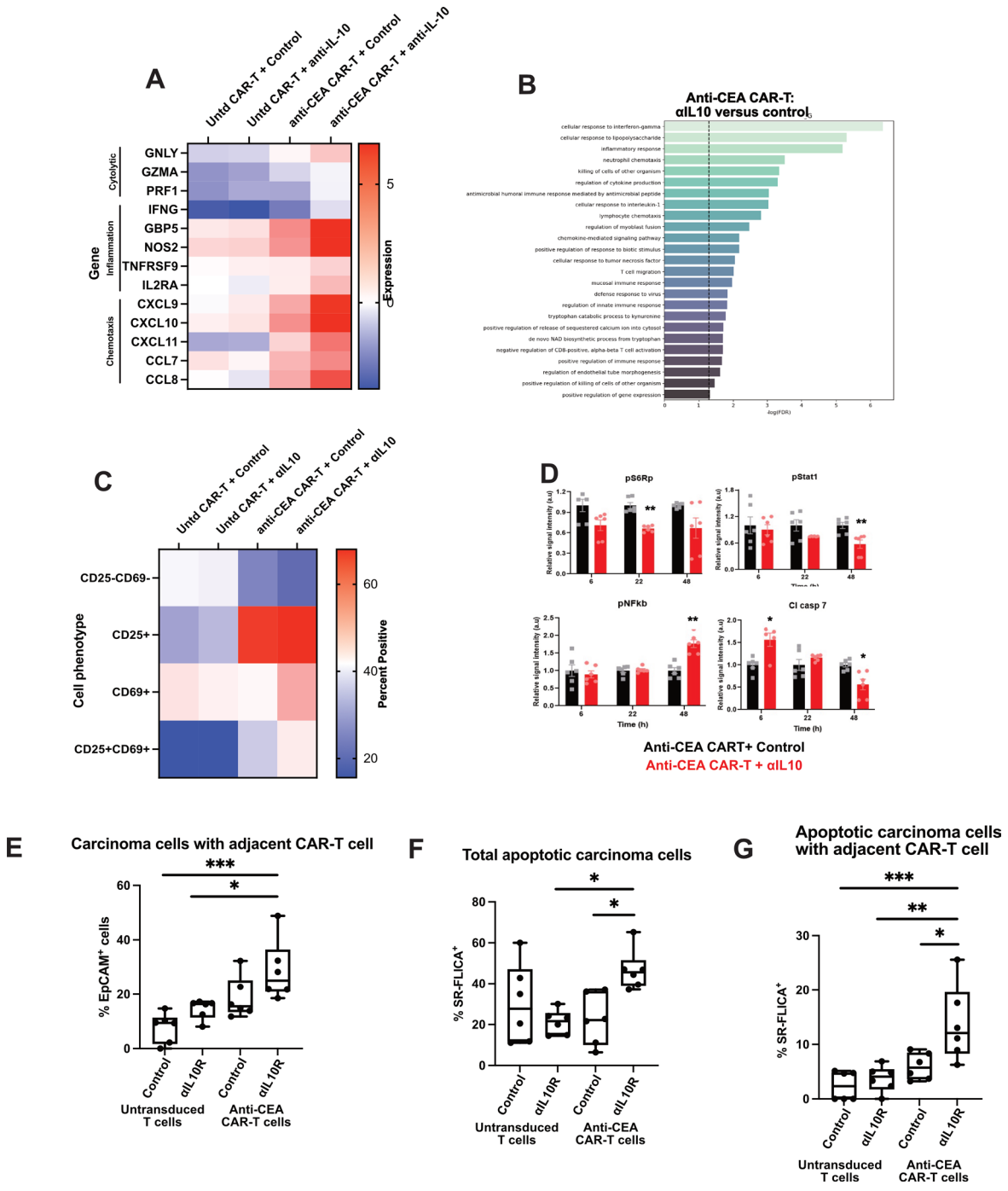

Figure 6 Interleukin 10 (IL-10) blockade increases antigen-specific chimeric antigen receptor T (CAR-T) cell activation through a mechanism that requires intact IL-10R on CAR-T cells. Human colorectal cancer liver metastases (CRLM) slices were treated with control or carcinoembryonic antigen (CEA)-specific CAR-T cells, plus control or αIL-10, for 1 day. (A) Tumour slices were analysed by bulk RNA sequencing with heatmap demonstrating expression of genes related to T cell cytolytic functioning, activation and migration/chemotaxis for each treatment group (n=2 tumours). Dark red denotes high expression of the listed gene and dark blue denotes comparably low expression normalised to housekeeping genes. (B) Gene expression pathways increased with anti-CEA CAR-T cells are treated with αIL-10 versus control. Untd, untransduced control CAR-T cells. (C) Representative case of flow cytometry performed on CAR-T cells after treatment with control or IL-10 blocking antibody demonstrating expression of CD25 and CD69 (n=2 tumours). (D) Reverse phase protein array showing expression of pS6, Stat1, nuclear factor kappa B (NF-κB) and cleaved Caspase-7 protein of slices treated with anti-CEA CAR-T cells and either control or αIL-10 at 6, 22 and 48 hours. After 6 hours, cleaved Caspase-7 expression is increased in the slices treated with the CAR-T in addition to αIL-10, and at 22 hours pS6 expression is decreased. After 48 hours, Stat1 and cleaved Caspase-7 are decreased with an increase in NF-κB. Each data point represents a replicate from n=2 cases. Student's t-test. *p<0.05; **p<0.01. (E–G) Following treatment of either untransduced control or anti-CEA CAR-T cells with either control or αIL-10R, the CAR-T cells alone were incubated with tumour slice culture and live imaging was performed. Again, quantification of the carcinoma cells with a CAR-T cell adjacent (defined as within 20 µm), total SR-FLICA$^+$ carcinoma cells and SR-FLICA$^+$ carcinoma cells with a CAR-T cell adjacent. Data points represent each high-powered fields (hpf) area imaged, with 3 hpf imaged in each tumour (n=3 separate human tumour samples). Analysis of variance with multiple comparisons. *p<0.05, **p<0.01, ***p<0.001.

models is essential to future clinical success. Using a unique human tumour-based model of metastatic CRC, we demonstrate that the immunosuppressive cytokine IL-10 is a pivotal mechanism of immune evasion in human CRLM. In a heterogeneous cohort of 38 unique patients' tumours, IL-10 blockade nearly doubled tumour apoptosis (figure 2C–E) through an immune-mediated mechanism dependent on both MHC class I and class II antigen presentation (figure 3G). The relevance of IL-10 in CRLM to antigen-specific T-cell function was further underscored by CAR-T cell experiments, in which αIL-10 dramatically increased proliferation and cytotoxicity of CEA-specific CAR-T cells in a murine cell coculture systems (figure 4) and human CRLM slice cultures (figures 5 and 6).

Combined, our data identify IL-10 as a major immune checkpoint to overcome in human CRLM and support a model in which IL-10 in the CRLM TME maintains MHC class II-low TAMs with poor antigen presenting capacity, resulting in ineffective cytotoxicity of tumour antigen-specific T cells. We found that blocking the effect of IL-10 in the TME results in reduced protein kinase B (AKT) and mitogen-activated protein kinase (MAPK) pathway phosphorylation, followed by increased MHC-II-dependent antigen presentation by macrophage, leading to $CD8^+$ T cell proliferation and activation, resulting in tumour cell death. It is perhaps due to either the relatively short duration of treatment (1 week) or to the presence of and help from $CD4^+$ T cells on $CD8^+$ T cells and the short culture period that despite T-cell activation, we do not see transcriptomic evidence of T cell exhaustion.[54] To test the effects of IL-10 and IL-10 blockade on antigen-specific T cells within the human CRLM environment, we modified the TSC system to include adoptive transfer of control or CEA-specific CAR-T cells. Although CAR-T recognise surface antigen through a different mechanism than the native T-cell receptor/peptide/MHC complex, adoptive CAR-T transfer was the most feasible approach within our heterogeneous human tumours. Within this modified system, we found that antagonism of IL-10 ligand or receptor caused rapid activation of antigen-specific CAR-T cells in the TME, with concurrent transcriptional and proteomic changes reflective of cytotoxic function (increased expression of *GBP5*, *NOS2*, *CXCL9*, *CXCL10* and *CCL8*) and T-cell activation (increased NF-κB expression and increased $CD25^+CD69^+$ population). Overall, these data suggest direct IL-10 effects via IL-10R signalling in both the myeloid and T-cell compartments in CRLM, inhibition of which leads to rapid changes in gene and protein expression in IL-10-target cells that culminate in immune-mediated tumour killing.

Our results provide a human cancer context for the large body of literature detailing the direct inhibitory effects of IL-10 on both APC and T-cell function.[18] In the context of liver-mediated tolerance,[19] we hypothesised that IL-10 might also inhibit APC and T-cell function in the liver TME. Our findings corroborate what others have demonstrated in the primary murine TME. A murine model of breast cancer demonstrated that macrophage-derived IL-10 suppressed DC production of IL-12, which was necessary for maximal $CD8^+$ T cell function and chemotherapy response.[22] In a flank tumour model of lung cancer, tumour growth was enhanced in transgenic mice overexpressing *Il10*, which was reversible with antibody-mediated IL-10 blockade.[55] Tumour monocyte-derived IL-10 was directly inhibitory on T-cell proliferation in an orthotopic murine model of CRC.[56] In the clinical context, a meta-analysis of 1788 patients spanning 10 different cancer types demonstrated correlation between serum IL-10 concentration and worse survival.[21] Together, these studies describe an immunosuppressive, protumoral effect of IL-10.

However, evidence also suggests that IL-10 paradoxically activates antigen-experienced T cells and induces immune-mediated tumour regression. PEGylated IL-10 (pegilodecakin, AM0010) has been shown to induce $CD8^+$ T cell-dependent tumour regression in a murine flank model of squamous cell carcinoma.[26] A phase I trial of pegilodecakin in advanced solid cancers demonstrated regression in 5/24 patients.[27] In responding patients, activated T cells expanded in both the peripheral blood and tumour and peripheral clonal T cell expansion coincided with delayed tumour response.[28] IL-10 in vitro increased granzyme B effector molecule expression in activated human peripheral blood $CD8^+$ T cells, and increased cytotoxicity of tumour-specific CAR-T cells cocultured with target human leukaemia cells.[57] An IL-10 fusion protein, IL-10-Fc, expanded and rescued terminally exhausted T cells in murine melanoma and CRC through metabolic reprogramming.[58] Together, these data provide an argument for potential immune-activating, antitumour effects of IL-10. However, two clinical trials of pegilodecakin in pancreatic cancer[34] and non-small cell lung cancer[35] did not meet prespecified endpoints.

The key to the IL-10 paradox likely relates to context, including stoichiometry, kinetics of ligand/receptor interactions and organ-specific immune environmental factors. Notably, the 3D structure of the active IL-10/IL-10RA/IL-10RB hexamer complex was recently defined. This informed design of IL-10 variants with varying receptor subtype affinity, allowing for cell type-specific induction of myeloid but not T cell IL-10R signalling.[33] A limitation of the current study is the cell type-indiscriminate effects of αIL-10. The requirement of both MHC class I and class II for maximal αIL-10 effect (figure 3G) demonstrates that both endogenous T cells and APC are required for optimal response, suggesting that more precise myeloid cell targeting could further enhance immune responses. Development of novel IL-10R antagonists and additional RNA-based methods of gene knockdown will enhance the TSC platform and help address these next-order questions.

Another limitation of the TSC model is the absence of circulating blood or draining lymph node components. In vivo murine models are a potential strategy to investigate the effects of systemic or regional lymphocytes, but must be interpreted with caution, given the limitations of carcinogen-derived, transplanted flank models, which are often more immunogenic than human cancer counterparts.[59 60] For example, one study in $IL\text{-}10^{-/-}$ mice with MC38 murine colon carcinoma cells demonstrated that IL-10 inhibited inflammatory cytokines and resulted in reduced tumour growth.[61] Specifically, the MC38 mouse model has been shown to represent MSI-high CRC,[62] which clinically in humans correlates with high tumour mutation burden (TMB) and response to ICI. However, most patients with metastatic CRC have MSS tumours with low TMB and do not respond to ICI; thus, modelling and designing new immunotherapeutic approaches for patients with MSS CRC is a major clinical need. The fact that αIL-10 is nevertheless able to elicit immune-mediated tumour regression is notable, given the complete reliance on immune cells present in a 6 mm diameter×250 µm-thick tumour slice. Our findings build on the foundation of profiled intratumoral T cells[8 63] and myeloid cells,[10] confirming the presence of T cells and APC capable of together mounting an antitumour response. Future work will investigate whether IL-10 blockade causes clonal $CD8^+$ and/or $CD4^+$ T-cell expansion and parallel studies will define the baseline and αIL-10-induced polarisation of TAMs. In CRLM slices, macrophages were a major source of IL-10 (figure 1B), yet IL-10 blockade significantly increased MHC class II expression (figure 3B; online

supplemental figure S3D). IL-10 blockade may therefore represent a novel approach to repolarising inhibitory macrophages in CRLM.

Given the safety of CAR-T therapy in CRLM in human clinical trials,[13 14] strategies to enhance adoptive cellular therapy are also needed. Here, we found that αIL-10 significantly increased CAR-T migration, proliferation and cytotoxicity in CRLM (figures 4–6). Our findings suggest that 'arming' CAR-T cells against IL-10, for example, through transgenic expression of a neutralising IL-10 antibody, may achieve the dual benefit of enhancing CAR-T function and serving as a novel delivery vehicle of IL-10 blockade. Interestingly, IL-10R blockade prior to adoptive transfer leads to similar results, indicating a direct mechanistic effect of IL-10 on the CAR-T cells (figure 6E–G). Future work will define molecular mechanisms underlying the rapid (<24 hours) response of CAR-T cells to αIL-10, such as downstream changes in STAT3 phosphorylation and expression. Given the paradoxical effects of IL-10 observed in leukaemia-specific CAR-T cells in vitro,[57] it will be important to define in which contexts, for example, liver metastases, optimal T-cell activation results from blockade rather than additional IL-10/IL-10R signalling.

The controversial role of IL-10 in cancer underscores the importance of studying this cytokine in accurate preclinical models that faithfully recapitulate human cancer. Here, we present evidence that IL-10 suppresses antitumour immunity in human CRLM and that a neutralising antibody against IL-10 can reverse this effect to induce dramatic immune-mediated tumour death. We previously demonstrated that TSC accurately recapitulates tumour and stromal elements of multiple GI carcinomas[35 37] and predicts patient responses to both standard chemotherapies[34] and novel immunotherapy combinations.[38] Despite limitations of human TSC, it is nevertheless notable that we observed a response in over two-thirds of patients' tumours, despite variability in tumour mutational status and preoperative chemotherapy response. We conclude that IL-10 is a major immune checkpoint to overcome in CRLM. Future work will investigate the relevance of IL-10 blockade to other primary and secondary liver tumours, and other immune-infiltrated tumours resistant to ICI.

Author affiliations
[1]Department of Surgery, University of Washington, Seattle, Washington, USA
[2]Immuno-Oncology Institute and Department of Medicine, Roger Williams Medical Center, Providence, Rhode Island, USA
[3]Department of Surgery, Boston University School of Medicine, Boston, Massachusetts, USA
[4]Institute for Systems Biology, Seattle, Washington, USA
[5]Brotman Baty Institute for Precision Medicine, Seattle, Washington, USA
[6]Human Biology Division, Fred Hutchinson Cancer Research Center, Seattle, Washington, USA
[7]Department of Pathology, University of Washington, Seattle, Washington, USA
[8]National Research Center for Translational Medicine, Ruijin Hospital Affiliated to Shanghai Jiao Tong University School of Medicine, Shanghai, China

Correction notice This article has been corrected since it published Online First. The author's name, Qiang Tian, has been corrected.

Twitter Kevin M Sullivan @kmsullivanmd, Teresa S Kim @TeresaKimMD and Venu G Pillarisetty @pancsurg

Acknowledgements This research was also supported by the Experimental Histopathology Shared Resource of the Fred Hutch/University of Washington Cancer Consortium (P30 CA015704). We acknowledge support from the National Institutes of Health (S10 OD016240) to the W. M. Keck Center for Advanced Studies in Neural Signaling and the assistance of Keck Center manager, Dr Nathaniel Peters. We thank Stella Shin and CB Lim for assistance with RPPA samples. We also thank Dr Jeffrey Schlom for the generous gift of MC38CEA cell line. The authors also thank Sorrento and TNK Therapeutics for generously preparing and providing the anti-CEA CAR-T cells and CEA-Fc detection reagent.

Contributors Conceptualisation: KMS, XJ, CL, HLK, VGP. Methodology: KMS, XJ, PG, CL, JAC, CH, KK, SKD, HLK, XY, CM, MC, YDS, TSK, TSG, RSY, QT, SCK, VGP. Investigation: KMS, XJ, PG, CL, CH, KPL, SKD, KK, CM, MC, HLK, AA. Visualisation: KMS, XJ, PG, CL, CH, KPL, SCK, KK, MC, HLK, AA, SKD, TSG, TSK, VGP. Funding acquisition: KMS, RSY, SCK, TSK, TSG, QT, SCK, VGP. Project administration: KMS, XJ, PG, CL, HLK, JOP, TSG, QT, SCK, VGP. Supervision: TSG, TSK, JOP, INC, RSY, SCK, VGP. Writing–original draft: KMS, PG, SCK, VGP. Writing–review and editing: KMS, XJ, PG, KPL, KK, CH, HLK, SKD, AA, YDS, TSG, TSK, JOP, INC, RSY, SCK, VGP. Guarantor: KMS, VGP.

Funding KMS received funding from the Fibrolamellar Cancer Foundation and Cancer Research Institute (FCF/CRI Postdoctoral Fellowship). TSG received funding from the American Cancer Society (RSG-19-197-01). TSK received funding from the UW/Fred Hutchinson Cancer Center Support Grant (CCSG), P30 CA015704, New Investigator Award. QT received funding from USAMRAA (CA150370P1) and NIH (NCI R01 CA190122). VGP and SCK received funding from the US Army Medical Research Acquisition Activity (USAMRAA; CA150370P2). RSY received funding from USAMRAA (CA150370). VGP received funding from Seattle Translational Tumor Research, Brotman Baty Institute for Precision Medicine, and Merck Investigator Studies Program.

Competing interests VGP is a member of the scientific advisory board for TriSalus Life Sciences. He has served as a consultant for Merck & Company in 2018, GlaxoSmithKline in 2019, Imvax in 2019, Takeda in 2020 and Umoja in 2022. He has research funding from AstraZeneca, Ipsen, Merck, OncoResponse and NGM. The funders had no role in the conceptualisation, design, data collection, analysis, decision to publish or preparation of the manuscript. The anti-CEA CAR vector was provided by TNK Therapeutics, who had no role in the conceptualisation, design, data collection, analysis or preparation of the manuscript. SCK served as an advisor for TNK Therapeutics until December 2019, is currently Chief Medical Officer of TriSalus Life Sciences and SAB member of Nkarta, Takeda and Sentibio, and has received research funding from Takeda and Nkata.

Patient and public involvement Patients and/or the public were not involved in the design, conduct, reporting or dissemination plans of this research.

Patient consent for publication Not required.

Ethics approval This study involves human participants and was approved by University of Washington Institutional Review Board (protocol no. 1852). Participants gave informed consent to participate in the study before taking part.

Provenance and peer review Not commissioned; externally peer reviewed.

Data availability statement Data are available in a public, open access repository. All data relevant to the study are included in the article or uploaded as supplementary information. Data from our RNA sequencing and single-cell RNAseq have been deposited and are available at https://doi.org/10.5061/dryad.0cfxpnw54.

ORCID iDs
Kevin M Sullivan http://orcid.org/0000-0001-7455-2308
Teresa S Kim http://orcid.org/0000-0002-6040-7748
Taranjit S Gujral http://orcid.org/0000-0002-4453-3031
Venu G Pillarisetty http://orcid.org/0000-0002-1162-9643

REFERENCES

1 Siegel RL, Miller KD, Fedewa SA, *et al*. Colorectal cancer statistics, 2017. *CA Cancer J Clin* 2017;67:177–93.
2 Engstrand J, Nilsson H, Strömberg C, *et al*. Colorectal cancer liver metastases - a population-based study on incidence, management and survival. *BMC Cancer* 2018;18:78
3 Koopman M, Kortman GAM, Mekenkamp L, *et al*. Deficient mismatch repair system in patients with sporadic advanced colorectal cancer. *Br J Cancer* 2009;100:266–73.
4 Topalian SL, Hodi FS, Brahmer JR, Safety BJR, *et al*. Safety, activity, and immune correlates of anti-PD-1 antibody in cancer. *N Engl J Med* 2012;366:2443–54.
5 Brahmer JR, Tykodi SS, Chow LQM, *et al*. Safety and activity of anti-PD-L1 antibody in patients with advanced cancer. *N Engl J Med* 2012;366:2455–65.

6 Lee JJ, Sun W, Bahary N. Phase 2 study of pembrolizumab in combination with azacitidine in subjects with metastatic colorectal cancer. *Journal of Clinical Oncology* 2017;35:3054–54.
7 Segal NH, Kemeny NE, Cercek A. Non-randomized phase II study to assess the efficacy of pembrolizumab (Pem) plus radiotherapy (RT) or ablation in mismatch repair proficient (pMMR) metastatic colorectal cancer (mCRC) patients. *Journal of Clinical Oncology* 2016;34:3539–39.
8 Wang Y, Lin H-C, Huang M-Y, *et al*. The immunoscore system predicts prognosis after liver metastasectomy in colorectal cancer liver metastases. *Cancer Immunol Immunother* 2018;67:435–44.
9 Katz SC, Bamboat ZM, Maker AV, *et al*. Regulatory T cell infiltration predicts outcome following resection of colorectal cancer liver metastases. *Ann Surg Oncol* 2013;20:946–55.
10 Donadon M, Torzilli G, Cortese N, *et al*. Macrophage morphology correlates with single-cell diversity and prognosis in colorectal liver metastasis. *J Exp Med* 2020;217. doi:10.1084/jem.20191847. [Epub ahead of print: 02 11 2020].
11 Cavnar MJ, Turcotte S, Katz SC, *et al*. Tumor-Associated macrophage infiltration in colorectal cancer liver metastases is associated with better outcome. *Ann Surg Oncol* 2017;24:1835–42.
12 Jin K-T, Chen B, Liu Y-Y, *et al*. Monoclonal antibodies and chimeric antigen receptor (CAR) T cells in the treatment of colorectal cancer. *Cancer Cell Int* 2021;21:83.
13 Zhang C, Wang Z, Yang Z, *et al*. Phase I Escalating-Dose Trial of CAR-T Therapy Targeting CEA$^+$ Metastatic Colorectal Cancers. *Mol Ther* 2017;25:1248–58.
14 Katz SC, Burga RA, McCormack E, *et al*. Phase I hepatic immunotherapy for metastases study of intra-arterial chimeric antigen receptor-modified T-cell therapy for CEA+ liver metastases. *Clin Cancer Res* 2015;21:3149–59.
15 Thorn M, Guha P, Cunetta M, *et al*. Tumor-Associated GM-CSF overexpression induces immunoinhibitory molecules via STAT3 in myeloid-suppressor cells infiltrating liver metastases. *Cancer Gene Ther* 2016;23:188–98.
16 Burga RA, Thorn M, Point GR. Liver myeloid-derived suppressor cells expand in response to liver metastases in mice and inhibit the anti-tumor efficacy of anti-CEA CAR-T. *Cancer Immunol Immunother* 2015;64:817–29.
17 Guha P, Gardell J, Rabinowitz B, *et al*. Monocytic and granulocytic myeloid-derived suppressor cell plasticity and differentiation are organ-specific. *Oncogene* 2021;40:693–704.
18 Saraiva M, Vieira P, O'Garra A. Biology and therapeutic potential of interleukin-10. *J Exp Med* 2020;217. doi:10.1084/jem.20190418. [Epub ahead of print: 06 01 2020].
19 Crispe IN. Hepatic T cells and liver tolerance. *Nat Rev Immunol* 2003;3:51–62.
20 Li B, Wang F, Ma C, *et al*. Predictive value of IL-18 and IL-10 in the prognosis of patients with colorectal cancer. *Oncol Lett* 2019;18:713–9.
21 Zhao S, Wu D, Wu P, *et al*. Serum IL-10 predicts worse outcome in cancer patients: a meta-analysis. *PLoS One* 2015;10:e0139598–e98.
22 Ruffell B, Chang-Strachan D, Chan V, *et al*. Macrophage IL-10 blocks CD8+ T cell-dependent responses to chemotherapy by suppressing IL-12 expression in intratumoral dendritic cells. *Cancer Cell* 2014;26:623–37.
23 Rossowska J, Anger N, Szczygieł A, *et al*. Reprogramming the murine colon cancer microenvironment using lentivectors encoding shRNA against IL-10 as a component of a potent DC-based chemoimmunotherapy. *J Exp Clin Cancer Res* 2018;37:126
24 Mocellin S, Panelli MC, Wang E, *et al*. The dual role of IL-10. *Trends Immunol* 2003;24:36–43.
25 Mannino MH, Zhu Z, Xiao H, *et al*. The paradoxical role of IL-10 in immunity and cancer. *Cancer Lett* 2015;367:103–7.
26 Mumm JB, Emmerich J, Zhang X, *et al*. Il-10 elicits IFNγ-dependent tumor immune surveillance. *Cancer Cell* 2011;20:781–96.
27 Naing A, Papadopoulos KP, Autio KA, *et al*. Safety, antitumor activity, and immune activation of PEGylated recombinant human interleukin-10 (AM0010) in patients with advanced solid tumors. *J Clin Oncol* 2016;34:3562–9.
28 Naing A, Infante JR, Papadopoulos KP, *et al*. PEGylated IL-10 (Pegilodecakin) Induces Systemic Immune Activation, CD8$^+$ T Cell Invigoration and Polyclonal T Cell Expansion in Cancer Patients. *Cancer Cell* 2018;34:775–91.
29 Chan IH, Wu V, Bilardello M, *et al*. PEG-rIL-10 treatment decreases FoxP3(+) Tregs despite upregulation of intratumoral IDO. *Oncoimmunology* 2016;5:e1197458.
30 Emmerich J, Mumm JB, Chan IH, *et al*. IL-10 directly activates and expands tumor-resident CD8(+) T cells without de novo infiltration from secondary lymphoid organs. *Cancer Res* 2012;72:3570–81.
31 Lilly Announces phase 3 study in patients with metastatic pancreatic cancer did not meet primary endpoint of overall survival 2019. Available: https://investor.lilly.com/news-releases/news-release-details/lilly-announces-phase-3-study-patients-metastatic-pancreatic [Accessed 1/7/20 2019].
32 Spigel D, Jotte R, Nemunaitis J, *et al*. Randomized phase 2 studies of checkpoint inhibitors alone or in combination with Pegilodecakin in patients with metastatic NSCLC (cypress 1 and cypress 2). *J Thorac Oncol* 2021;16:327–33.
33 Saxton RA, Tsutsumi N, Su LL, *et al*. Structure-Based decoupling of the pro- and anti-inflammatory functions of interleukin-10. *Science* 2021;371. doi:10.1126/science.abc8433. [Epub ahead of print: 19 03 2021].
34 Jabbari N, Kenerson HL, Lausted C, *et al*. Modulation of immune checkpoints by chemotherapy in human colorectal liver metastases. *Cell Rep Med* 2020;1:100160.
35 Jiang X, Seo YD, Chang JH, *et al*. Long-Lived pancreatic ductal adenocarcinoma slice cultures enable precise study of the immune microenvironment. *Oncoimmunology* 2017;6:e1333210.
36 Jiang X, Seo YD, Sullivan KM. Establishment of slice cultures as a tool to study the cancer immune microenvironment. *Methods Mol Biol* 1884;2019:283–95.
37 Seo YD, Jiang X, Sullivan KM, *et al*. Mobilization of CD8$^+$ T Cells via CXCR4 Blockade Facilitates PD-1 Checkpoint Therapy in Human Pancreatic Cancer. *Clin Cancer Res* 2019;25:clincanres.0081.2019.
38 Bockorny B, Semenisty V, Macarulla T, *et al*. BL-8040, a CXCR4 antagonist, in combination with pembrolizumab and chemotherapy for pancreatic cancer: the combat trial. *Nat Med* 2020;26:878–85.
39 Goldman M, Craft B, Hastie M. The UCSC Xena platform for public and private cancer genomics data visualization and interpretation. *bioRxiv* 2019.
40 Kenerson HL, Sullivan KM, Labadie KP, *et al*. Protocol for tissue slice cultures from human solid tumors to study therapeutic response. *STAR Protoc* 2021;2:100574.
41 Luckert K, Gujral TS, Chan M, *et al*. A dual array-based approach to assess the abundance and posttranslational modification state of signaling proteins. *Sci Signal* 2012;5:pl1.
42 Gujral TS, Karp RL, Finski A, *et al*. Profiling phospho-signaling networks in breast cancer using reverse-phase protein arrays. *Oncogene* 2013;32:3470.
43 Lausted C, Sullivan KM, Guha P. Colorectal cancer interleukin-10 blockade scRNA-seq. *Dryad Digital Repository* 2022.
44 Burga RA, Thorn M, Point GR, *et al*. Liver myeloid-derived suppressor cells expand in response to liver metastases in mice and inhibit the anti-tumor efficacy of anti-CEA CAR-T. *Cancer Immunol Immunother* 2015;64:817–29.
45 Le DT, Uram JN, Wang H, *et al*. Pd-1 blockade in tumors with mismatch-repair deficiency. *N Engl J Med* 2015;372:2509–20.
46 Wherry EJ, Kurachi M. Molecular and cellular insights into T cell exhaustion. *Nat Rev Immunol* 2015;15:486–99.
47 Simon S, Vignard V, Florenceau L, *et al*. Pd-1 expression conditions T cell avidity within an antigen-specific repertoire. *Oncoimmunology* 2016;5:e1104448.
48 Gros A, Robbins PF, Yao X, *et al*. Pd-1 identifies the patient-specific CD8$^+$ tumor-reactive repertoire infiltrating human tumors. *J Clin Invest* 2014;124:2246–59.
49 Tretina K, Park E-S, Maminska A, *et al*. Interferon-Induced guanylate-binding proteins: guardians of host defense in health and disease. *J Exp Med* 2019;216:482–500.
50 Tokunaga R, Zhang W, Naseem M, *et al*. CXCL9, CXCL10, CXCL11/CXCR3 axis for immune activation - A target for novel cancer therapy. *Cancer Treat Rev* 2018;63:40–7.
51 Hopewell EL, Zhao W, Fulp WJ, *et al*. Lung tumor NF-κB signaling promotes T cell-mediated immune surveillance. *J Clin Invest* 2013;123:2509–22.
52 Gerondakis S, Siebenlist U. Roles of the NF-kappaB pathway in lymphocyte development and function. *Cold Spring Harb Perspect Biol* 2010;2:a000182.
53 Philipson BI, O'Connor RS, May MJ, *et al*. 4-1Bb costimulation promotes CAR T cell survival through noncanonical NF-κB signaling. *Sci Signal* 2020;13. doi:10.1126/scisignal.aay8248. [Epub ahead of print: 31 03 2020].
54 Borst J, Ahrends T, Bąbała N, *et al*. CD4$^+$ T cell help in cancer immunology and immunotherapy. *Nat Rev Immunol* 2018;18:635–47.
55 Hagenbaugh A, Sharma S, Dubinett SM, *et al*. Altered immune responses in interleukin 10 transgenic mice. *J Exp Med* 1997;185:2101–10.
56 Jung K, Heishi T, Khan OF, *et al*. Ly6Clo monocytes drive immunosuppression and confer resistance to anti-VEGFR2 cancer therapy. *J Clin Invest* 2017;127:3039–51.
57 Gorby C, Sotolongo Bellón J, Wilmes S, *et al*. Engineered IL-10 variants elicit potent immunomodulatory effects at low ligand doses. *Sci Signal* 2020;13. doi:10.1126/scisignal.abc0653. [Epub ahead of print: 15 09 2020].
58 Guo Y, Xie Y-Q, Gao M, *et al*. Metabolic reprogramming of terminally exhausted CD8$^+$ T cells by IL-10 enhances anti-tumor immunity. *Nat Immunol* 2021;22:746–56.
59 Guerin MV, Finisguerra V, Van den Eynde BJ, *et al*. Preclinical murine tumor models: a structural and functional perspective. *Elife* 2020;9. doi:10.7554/eLife.50740. [Epub ahead of print: 28 Jan 2020].
60 Zhong W, Myers JS, Wang F, *et al*. Comparison of the molecular and cellular phenotypes of common mouse syngeneic models with human tumors. *BMC Genomics* 2020;21:2.
61 Tanikawa T, Wilke CM, Kryczek I, *et al*. Interleukin-10 ablation promotes tumor development, growth, and metastasis. *Cancer Res* 2012;72:420–9.
62 Efremova M, Rieder D, Klepsch V, *et al*. Targeting immune checkpoints potentiates immunoediting and changes the dynamics of tumor evolution. *Nat Commun* 2018;9:32.
63 Van den Eynde M, Mlecnik B, Bindea G, *et al*. The link between the Multiverse of immune microenvironments in metastases and the survival of colorectal cancer patients. *Cancer Cell* 2018;34:1012–26.

SUPPLEMENTARY MATERIALS:

Fig. S1.

Correlation of the highest and lowest quartiles of IL-10 expression with disease-specific survival (DSS) at 5 years in the TCGA Pan-Cancer of primary colon adenocarcinoma (COAD) dataset demonstrating improved DSS for colon cancer with low *IL10* expression ($P<0.05$), but no change in DSS for colon cancer for high vs low *PDCD1* and *HAVCR1*expression ($P>0.05$).

Fig. S2.

S2A – IL-10 cytokine was measured in TSC supernatant from n=5 tumors treated with control or αIL-10, with a marked reduction in the IL-10 detectable within the system.

S2B – Co-staining of IHC by EpCAM marking for tumor cells (red) and cleaved-Caspase-3 (CC3) for apoptotic cells (brown) indicates that the increased CC3 expression is occurring on tumor cells. $EpCAM^+$ $CC3^+$ cells are denoted with black arrows. Representative of n = 3 patient tumors.

S2C –Staining of consecutive slides of CD163 and HLA-DR. Cells positive in the same position on the consecutive slides are denoted by black arrows. Representative of n = 3 patient tumors.

S2D - Multiplex IHC was performed for T cells (CD3, green), PD-1 (red), and nuclei (DAPI, blue). Quantification of proportion of $PD\text{-}1^+$ $CD3^+$ cells are also shown (n = 6 patient tumors). Granzyme B^+ by tissue area similarly stained by IHC and quantified. Scale bar = 50 µm. Data points represent each human tumor sample. Student's t test.

Fig. S3.

Two separate patient tumors were collected on sequential days 1, 2, and 3 of treatment with IL-10 blocking antibody or control antibody. Single cell RNA sequencing was performed on all samples. Violin plots of gene expression of cytolytic and activation gene signatures in the in $CD8^+$ and $CD4^+$ T cell subsets as well as TAM subset. The activation gene signature consists of *CD69*, *FASLG*, *CD27*, *CD28*, *TNFRSF9*, *TNFRSF4*, *LAMP1*, *EOMES*, *TBX21*(A-B). The exhausted gene signature consists of *PDCD1, CTLA4, HAVCR2, TIGIT*, and *LAG3* (C). Last, violin plot of the MHC-II presentation genes in the Reactome pathway in the macrophage cell cluster (D).

Fig. S4.

Results of low dose (10^5 rather than 10^6) CAR-T cell showing similarly increased CAR-T cell migration and CAR-T cell mediated carcinoma cell apoptosis which did not meet statistical significance.

Fig. S5.

Representative flow cytometry plot and quantification of cells gated for $CFSE^+$ T cells which are also positive for CD25 and/or CD69 from experiments depicted in Fig. 6C.

Sullivan KM, *et al. Gut* 2022;0:1–13. doi: 10.1136/gutjnl-2021-325808

Supplemental Materials and Methods

Tumor slice culture

Slice culture of freshly resected human CRLM tumors was performed as previously described [35 36 40]. Briefly, sterile cores from tumor specimens were obtained using a 6 mm punch biopsy in the operating room immediately following resection, under the review of the on-call surgical pathologist to ensure the retention of adequate tissue for diagnosis and margin assessment. The cores were placed in Belzer UW Cold Storage solution on ice. Using a vibratome (Leica Biosystems), 250 µm slices were cut sequentially and placed on a permeable PTFE membrane with 0.4 µm pores (Millicell, MilliporeSigma, Burlington, MA), placed in a 24-well dish containing RPMI media with 10% fetal bovine serum (FBS) and 1% penicillin/streptomycin but without any additional immune-activating factors or cytokines. Slice cultures were incubated overnight at 37°C and then treated with 10% FBS RPMI media containing either 20 µg/mL of IgG isotype control (#553447, BD Biosciences), 20 µg/mL of αPD-11 (#562138, Biolegend), or 20 µg/mL of αIL-10 (#501407, Biolegend) For an individual tumor sample, slices were distributed evenly and randomly from throughout the tumor with 3 slices per treatment group to account for confounding from intra-tumor heterogeneity. Slices were only excluded for technical failure of slicing and no treated slices were excluded. Treatment samples were not blinded when analyzing results. The dose of αIL-10 was chosen based upon a dose titration experiment using 5, 10, and 20 µg/ml concentrations of antibody, showing a maximal effect at 20 µg/ml. Additional experiments used 20 µg/mL of anti-MHC class I (purified mouse anti-human HLA-ABC #555551, BD Biosciences) and/or 20 µg/mL of anti-MHC class II (purified mouse anti-human HLA-DR, DP, DQ #555557, BD Biosciences). If the slices were to be maintained in culture for more than 3 days, half the volume of media was changed with fresh treatment after 72 hours.

In situ hybridization (ISH) and multicolor immunohistochemistry (mIHC)

For ISH, FFPE tissues were sectioned at 4 µm onto positively-charged slides and baked for 1 hour at 60°C. The slides were then dewaxed and stained on a Leica BOND Rx Stainer (Leica, Buffalo Grove, IL) using Leica Bond reagents for dewaxing (Dewax Solution), antigen retrieval with Epitope Retrieval Solution 2 for 15 minutes at 95°C, cell permeabilization with 0.5% Triton-X in PBS for 30 minutes at RT and rinsing after each step (Bond Wash Solution). All steps after epitope retrieval were performed at RT. The slides were then blocked with hydrogen peroxide for 10 minutes and incubated with the ACD target probe, IFN-g (#550478-C3, Advanced Cell Diagnostics) or IL10Ra (#498058, Advanced Cell Diagnostics) and IL10 (#602058-C2, Advanced Cell Diagnostics), at 42°C for 120 minutes. After the probe incubation, the staining proceeded with the ACD RNAscope LS Multiplex Fluorescent Reagent Kit (#322800) for the amplification and detection steps, followed by Opal fluor (Opal 650 for IFN-g, Opal 570/650 for IL10RA/IL10) at 1:750 for 10 minutes. Slides were removed from the Stainer and stained with DAPI for 5 minutes, rinsed for 5 minutes, and a coverslip was mounted with Prolong Gold Antifade reagent (Invitrogen/Life Technologies, Grand Island, NY). Slides were imaged with Leica SP8 confocal microscope.

For the mIHC staining, the coverslip of slides was removed in deionized water and stained on a Leica BOND Rx using Leica Bond reagents for dewaxing (Dewax Solution), antibody stripping (Epitope Retrieval Solution 2), and rinsing after each step (Bond Wash Solution). Antibody stripping steps were performed at 100°C with all other steps at ambient temperature. Endogenous peroxidase was blocked with 3% H_2O_2 for 5 minutes followed by protein blocking with TCT buffer (0.05M Tris, 0.15M NaCl, 0.25% Casein, 0.1% Tween 20, 0.05% ProClin300 pH 7.6) for 10 minutes. The first

primary antibody (position 1) was applied for 60 minutes followed by the secondary antibody application for 10 minutes and the application of the tertiary TSA-amplification reagent (PerkinElmer OPAL fluor) for 10 minutes. The primary antibodies used were EpCAM (Opal 690, 32402, Biolegend) in position 1, HLA-DR (Opal 620, M0746, Dako) in position 2, CD3 (Opal 570, RM9107, ThermoFisher) in position 3, and CD163/68 (Opal 540, BSB3276, BioSB and M0876, Dako) in position 4 followed by the Powervision Mouse-HRP secondary antibody (Leica). A high stringency wash was performed after the secondary and tertiary applications using high-salt TBST solution (0.05M Tris, 0.3M NaCl, and 0.1% Tween-20, pH 7.2-7.6). Polymer HRP was used for all secondary applications, as specified in the table. The primary and secondary antibodies were stripped with retrieval solution for 20 minutes before repeating the process with the second primary antibody (position 2) starting with a new application of 3% H_2O_2. The process was repeated until all positions were completed; however, there was no stripping step after the final position. Slides were removed from the stainer and stained with DAPI for 5 minutes, rinsed for 5 minutes, and coverslip mounted with Prolong Gold Antifade reagent (Invitrogen/Life Technologies, Grand Island, NY). Slides were imaged with Leica SP8 confocal microscope.

For combination of mIHC and ISH mIHC staining was done either before or after ISH. Slides were imaged after each step. ISH labeling was bleached when mIHC was performed subsequently. To combine the signals from ISH and mIHC, images were overlaid, and areas of perfect nuclear overlap were analyzed. Images were analyzed using Imaris (Bitplane). Parameters for each segmented cell including area, sphericity, mean intensity values were exported as comma separated value (CSV) files. Mean intensity values were normalized via z-score normalization. CSV files were analyzed via Flowjo (Beckton Dickinson).

Reverse phase protein array (RPPA)

Protein microarrays were printed and processed as described previously [41 42]. Briefly, tumor slices were lysed in 2% SDS lysis buffers as described previously[41 42]. Tumor slice lysates were printed onto 16-pad nitrocellulose coated slides (Grace Biolabs, OR, US) using Aushon 2470 microarrayer (Aushon BioSystems, MA, US). Each sample was printed in duplicate, and slides were stored at – 20°C until processing. Slides were then washed 2-3 times with PBS for 5 min each and blocked with Odyssey Blocking Buffer (OBB, Licor, NE, USA) for one hour at room temperature. After blocking, arrays were incubated with primary antibodies in OBB at 4°C overnight. The next day, arrays were washed thrice with PBS and incubated with IRDye labeled secondary antibodies in OBB for 1 hour at room temperature. Following incubation, slides were scanned using Licor Odyssey CLX Scanner (LiCOR). Total signal intensity from each spot was quantified using Array-Pro analyzer software package (Media Cybernetics, MD, USA). The measurement of a specific protein from an individual sample was normalized to total beta-actin (Sigma, Cat #A1978).

Immunohistochemistry (IHC)

At the desired times following treatment, slices were removed from culture and fixed in 10% formalin. Tissue was then paraffin embedded and 4 µm thick tissue slices were mounted on slides for storage. Slides were de-paraffinized in xylene and rehydrated through graded ethanol followed by heat mediated antigen retrieval using 10 mM Sodium Citrate Buffer (pH 6.0) and blocked with 3% hydrogen peroxide for 5 minutes and Background Buster (Innovex Biosciences) for 30 minutes. IHC was performed via incubations with one primary antibody at 4°C overnight followed by host-matched secondary polymer reagent and color substrate. Primary antibodies used were as follows: CD8 (M7103, Dako), HLA-DR

(M0746, Dako), CD163 (ab189915, Abcam), and cleaved-Caspase-3 (#9661, Cell Signal Technologies). Secondary reagents were ImmPress Rabbit HRP and Mouse HRP (Vector Laboratories). Color development was performed using DAB Quanto (Brown HRP; Fisher Scientific). Slides were counterstained with Harris hematoxylin (Sigma) as appropriate, dehydrated, and mounted. The transversely cut slides were imaged over multiple 20x hpf to visualize the entire thickness of the slice.

For dual-color IHC staining, sections were first stained as above with a primary antibody against cleaved-Caspase-3 (#9661, Cell Signal Technologies) and host-match secondary antibody Immpress Rabbit HRP (Vector Laboratories). Color development was performed using DAB Quanto (Brown HRP; Fisher Scientific). Slides were washed with TBST and PBS washing buffers, re-blocked with Background Buster for 15 minutes, and re-incubated with EpCAM (ab124825, Abcam) as the primary antibody. Immpress alkaline phosphatase (AP) anti-rabbit polymer (Vector Laboratories) was then used as secondary antibody and color development was performed with Warp Red substrate (WR 806CHC, Biocare). Slides were washed with TBST and PBS and counterstained with Harris hematoxylin (Sigma) and directly mounted with Aqua-mount (13800, Lerner Laboratories).

Stained tissue sections were digitally scanned and uploaded to NanoZoomer Digital Pathology (Hamamatsu) image viewing software. Images we exported and positive DAB cells and hematoxylin-stained nuclei were visually counted using Fiji ImageJ software. Each data point represents one case consisting of multiple (at least 2) slices and a minimum of 2 hpf within a single slice to account for both intra- and inter-tumoral heterogeneity.

Mice, liver metastasis (LM) in vivo model and myeloid cell isolation

C57BL/6 male mice (6–8-week-old) obtained from Jackson Laboratories were bred and maintained under pathogen free conditions at Roger Williams Medical Center (RWMC) animal facility. All surgical procedures were approved by RWMC Institutional Animal Care and Use Committee (IACUC). To generate LM, mice were anesthetized and injected with $2.5x10^6$ MC38CEA (generous gift from Dr. Jeffrey Schlom) via spleen followed by splenectomy to confine metastases to the liver. Liver non-parenchymal cells were isolated from LM, four days post-tumor generation, as previously described[15]. Immunomagnetic beads against CD11b were used to purify bulk hepatic MDSCs (Miltenyi Biotech). Typical purity of beaded $CD11b^+$ cells were 80–90% from mice with LM.

CAR-T generation, proliferation assay and cytotoxicity assay

CAR-T cells were generated from mouse splenocytes as described previously[43] and MC38CEA cells were used as target tumor cells. Isolated myeloid cells were isolated from LM tumor bearing mice livers. CAR-T cells were carboxyfluorescein diacetate succinimidyl ester (CFSE, Life Technologies) labeled as per company's protocol. MC38CEA cells were plated at $2x10^4$ cells/well in 96-well cell culture plate (BD Bioscience) with myeloid cells + CAR-T cells in a 1:1:1 ratio. Cells were treated with 100ng/ml or 200 ng/ml and 400 ng/ml of IL-10 antibody (JES5-2A5, Biolegend). After 24 hours, cells were removed and analyzed for CFSE using flow cytometry. Supernatant was collected and analyzed for LDH as per manufacturer's protocol (Promega). No exclusion of data points was necessary and treatment groups were not able to be blinded during analysis. N = 3 biological replicates and n = 4 technical replicates were performed.

Flow cytometry

Antibodies specific for the following markers were used: CD3 (17A2, BD Bioscience), IL-10 (JES5-16E3, BD Bioscience), IL-10R (1B1.3a, Biolegend), CD11b (M1/70, BD Bioscience), Gr1 (RB6-8C5, Biolegend), and anti-idiotypic CEA-Fc (Sorrento Therapeutics). For human CAR-T cells, cells were stained for CFSE, CD25 (BD Bioscience, 560989) and CD69 (Invitrogen, 25069941). For intracellular staining, the BD Bioscience Fixation/Permeabilization kit was used. Unstained and isotype controls were used for gating purposes. Cells were collected for analysis using Cytoflex LX (Beckman Coulter) and post-acquisition analysis was performed using FlowJo software (BD Bioscience).

Live imaging

CRLM tumor slices cultures were created as described above. Untransduced control or CAR-T cells were thawed, washed, and stained with CFSE at a concentration of 0.5 mM. One million of the stained control or antigen-specific CAR-T cells were added on top of slices to be treated in culture followed by either control or αIL-10 to the supernatant added to the media, and slices with CAR-T cells and antibody treatment were incubated for 1 day. Treatment 10^5 CAR-T cell resulted in similar but non-significant results compared to 10^6 (Fig. S4). The treated CRLM tumor slices were transferred into fresh media in a 48 well plate with 10 mg/mL Alexa 647 EpCAM antibody to stain tumor cells (Biolegend, San Diego, CA) and SR-FLICA reagent to stain apoptotic cells per the manufacturer's instructions (ImmunoChemistry Technologies, Bloomington, MN) and were incubated for 3 hours at 37°C for staining. The slices were then stained for nuclei using 10 mg/mL Hoechst 33342 (ImmunoChemistry Technologies) for 10 min. The slices were washed twice with PBS and returned with their original media containing the CAR-T cell and antibody treatment to an 8-well culture slide (Ibidi USA, Fitchburg, WI) for imaging. Tissue culture conditions were maintained as close to cell culture incubator as possible while imaging was performed, by using a heated covered stage (PeCon,

Erbach, Germany) to 37°C while flushing warmed, humidified CO_2 through the enclosure. The slices were imaged using a Leica SP8X confocal microscope (Leica Microsystems, Wetzlar, Germany) at 20x magnification. For each treated slice, images were collected for 1 hour at three different positions throughout the slice with a z-stack of 20 μm. One slice was used per treatment group per patient given imaging constraints with random sequential slices assigned to each treatment group.

In an experiment blocking the IL-10R on CAR-T, the CAR-T were thawed and incubated overnight in tissue culture media with 20 mg/mL of either control or αIL-10R. The CAR-T cells were washed with PBS, spun, and resuspended in media. They were stained with CFSE and placed directly into the CRLM tissue slice culture media without additional treatment or antibody blockade. After 1 day, slices were stained and imaged as above.

No slices or data were excluded from analysis. Treatment groups were unable to be blinded for imaging or analysis. Image processing and data analysis were performed on Leica LAS X software (Leica Microsystems, Wetzlar, Germany) and Imaris software (Bitplane USA, Concord, MA). The data and images obtained were visualized using a maximum intensity projection of the 20 μm z-stack. The $EpCAM^+$, $CFSE^+$, $SR\text{-}FLICA^+$ cells were counted manually. All cells observed throughout the time imaged at each position in each slice were counted.

Bulk RNA sequencing

CRLM slice culture treated with either untransduced or anti-CEA CAR-T cells either with or without IL-10 blocking antibody as described above. RNA was extracted from slices using Qiagen RNEasy kit

per the manufacturer's instructions. Samples were submitted to the Northwest Genomics Center for NGS sequencing.

Single cell RNA sequencing (scRNAseq)

Tumor slice dissociation

Tumor slices were dissociated using the MACS Tumor Dissociation Kit (MiltenyiBiotec, Auburn, CA) according to the manufacturer's "dissociation of soft tumors" protocol. Prior to dissociation, an enzyme mix was prepared by adding fresh aliquots of enzymes A, R and H with the recommended volumes to RPMI 1640 medium in a sterile "gentleMACS C" tube. The initial mechanical dissociation step was performed by running the "h_tumor_01 program." Slices were then incubated at 37°C for 20-30 minutes under continuous rotation using the MACSmix Tube Rotator followed by a second mechanical dissociation step, "h_tumor_02 program". Slices were then visually evaluated and tubes were incubated for an additional 20 minutes at 37◦ C if undissociated tissue was visible. Slice tissue was further dissociated by running the "h_tumor_03" program. After a short spin, the cell suspension was passed through a 70 µm MACS SmartStrainer. The strainer was washed with a solution of 0.04% (w/v) molecular biology grade BSA (Gemini Bio Products) in PBS. Finally, the cell suspension was strained through a 30 µm MACS SmartStrainer. Cells were spun down at 300×g and supernatant was removed.

Removal of dead cells from single cell suspension

Dead cells were removed from single cell suspensions with the Dead Cell Removal kit (MiltenyiBiotec) and according to the Dead Cell Removal Rev B protocol (10X Genomics, Pleasanton, CA). Cells were resuspended in Dead Cell Removal MicroBeads and incubated for 15 minutes at room temperature. Meanwhile, an MS column (MiltenyiBiotec) was rinsed with binding buffer. The cell suspension was then diluted and applied to the MS column on a MiniMACS separator. The effluent containing the live

single cells in binding buffer was collected into sterile tubes. The binding buffer was then replaced with PBS containing 0.04% BSA through two wash steps. Wide-bore pipette tips (Rainin, Columbus, OH) were used to ensure minimum damage to single cells.

Single cell suspension preparation for 10X Genomics Single Cell experiments

The cell suspension was mixed with Trypan Blue, quantified with a Countess Automated Cell Counter (Life Technologies, Waltham, MA), and confirmed with a hemocytometer. Based on the cell concentration and the targeted cell recovery, the corresponding volume of cell suspension was mixed with nuclease free water and loaded on the Chromium Controller according to the Chromium Single Cell 3' Reagent Kits v2 protocol (10X Genomics). On average, 17,000 cells in 33.8 µl were loaded into each Chromium droplet generation microfluidic device to target the maximum cell recovery number of 10,000.

10X Droplet Sequencing

Cellular suspensions were loaded on a Chromium instrument (10X Genomics, San Francisco, CA) to generate single-cell Gelbead-In-EMulsion (GEM) droplets. Reverse transcription (RT) was performed in a C1000 Touch thermocycler (Biorad, Hercules, CA). After RT, GEMs were harvested and the cDNAs were amplified and cleaned with SPRIselect Reagent Kit (Beckman Coulter, Brea, CA). Indexed sequencing libraries were constructed using the Chromium Single-Cell 3' Library Kit (version 2) for enzymatic fragmentation, end-repair, A-tailing, adapter ligation, ligation cleanup, sample index PCR, and PCR cleanup. The barcoded sequencing libraries were quantified by quantitative PCR using the KAPA Library Quantification Kit (KAPA Biosystems, Wilmington, MA). Sequencing libraries were loaded on a NextSeq500 (Illumina, San Diego, CA) and run 150 cycles (26 bp for Read 1 and 124 bp for Read 2). Two indexed (multiplexed) libraries (i.e. Control, anti-IL-10) were loaded on to one flowcell to obtain a sequencing depth of approximately 100,000 reads per cell. Reads were aligned to

the human genome (GRCh38) and quantified using the Cell Ranger (version 2.0, http://cf.10xgenomics.com/releases/cell-exp/ cellranger-2.0.0.tar.gz). Poor-quality cells/GEMs, defined as those expressing a high proportion (>10%) of mitochondrial genes or a low number of total genes (<200) were discarded. Unique transcripts were identified by 10X unique molecular indexes (UMIs). UMI counts were normalized by adjusting for library size and dividing by the median count of each cell, as implemented by the Cell Ranger R kit (version 2.0, http://cf.10xgenomics.com/supp/cell-exp/¬rkit-install-2.0.0.R).

Cell type classification and clustering

Sample UMI data were aggregated and the gene-cell matrix was normalized to give each gene a mean of 0 and standard deviation of 1. Principal Component Analysis was performed, and the top 30 components used to calculate a Uniform Manifold Approximation and Projection (UMAP) for visualization of all single cells in a two-dimensional space. Cells were clustered by the Leiden algorithm (26) as implemented with the SCANPY toolkit (27).

Table S1 – treatment antibodies

Antibody	**Manufacturer**	**Catalog no.**
Monoclonal IgG	BD Biosciences	#553447
Anti-IL-10	Biolegend	#501407
Anti-PD-1	BD Biosciences	#562138
Anti-MHC I	BD Biosciences	#555551
Anti-MHC II	BD Biosciences	#555557

Table S2 – ISH probes, mIHC antibodies, and live fluorescent imaging antibodies**Antibody**	**Fluorophore**	**Manufacturer**	**Catalog no.**
IFNG	Opal 650	Advanced Cell Diagnostics	#550478-C3
IL10RA	Opal 570	Advanced Cell Diagnostics	#498058
IL10	Opal 650	Advanced Cell Diagnostics	#602058-C2
EpCAM	Opal 690	Biolegend	32402
HLA-DR	Opal 620	Dako	M0746
CD3	Opal 570	ThermoFisher	RM9107
CD163	Opal 540	BioSB	BSB3276
CD68	Opal 540	Dako	M0876
EpCAM	Alexa 647	Biolegend	324212
Poly caspases	SR-FLICA	ImmunoChemistry Technologies	916

Table S3 – IHC antibodies

Antibody	**Manufacturer**	**Catalog no.**
cleaved-Caspase-3	Cell Signal Technologies	#9661
CD163	Abcam	ab189915
HLA-DR	Dako	M0746
CD4	Dako	M7310
CD8	Dako	M7103

Table S4 – flow cytometry antibodies

Antibody	**Manufacturer**	**Catalog no.**
CD3	BD Bioscience	17A2
IL-10	BD Bioscience	JES5-16E3
IL-10R	Biolegend	1B1.3a
CD11b	BD Bioscience	M1/70
Gr1	Biolegend	RB6-8C5
anti-idiotypic CEA-Fc	Sorrento Therapeutics	
CD69	Invitrogen	25069941
CD25	BD Bioscience	560989

S1

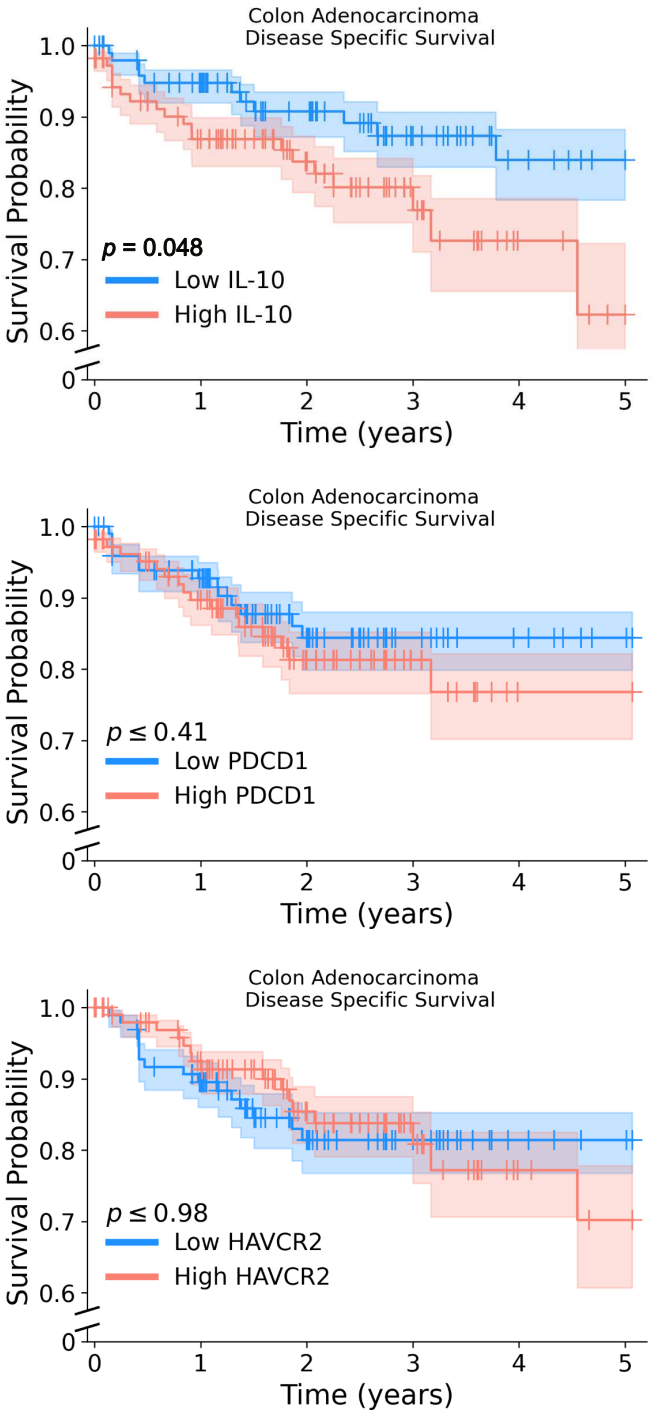
Colon Adenocarcinoma
Disease Specific Survival
Survival Probability
1.0
0.9
0.8
0.7
0.6
0
p = 0.048
Low IL-10
High IL-10
0
1
2
3
4
5
Time (years)
Colon Adenocarcinoma
Disease Specific Survival
Survival Probability
p ≤ 0.41
Low PDCD1
High PDCD1
Time (years)
Colon Adenocarcinoma
Disease Specific Survival
Survival Probability
p ≤ 0.98
Low HAVCR2
High HAVCR2
Time (years)

S2A

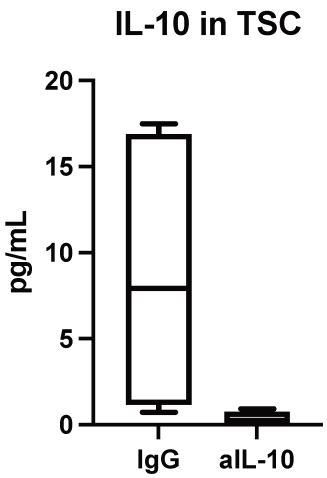

S2B

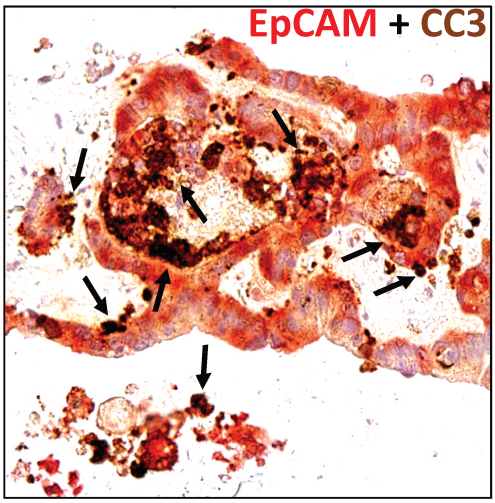

S2C

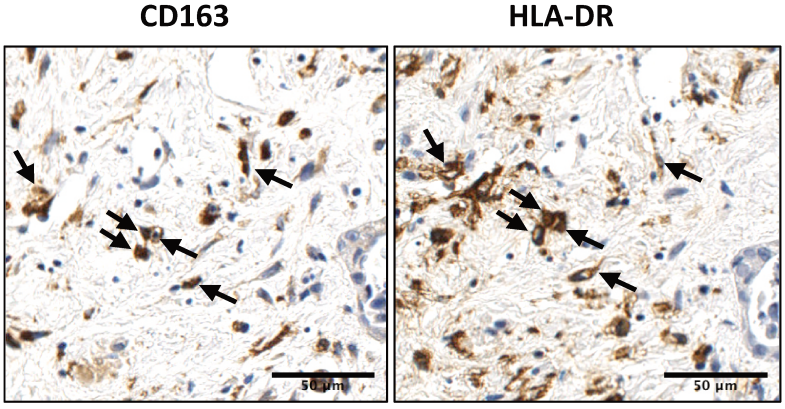

S2D

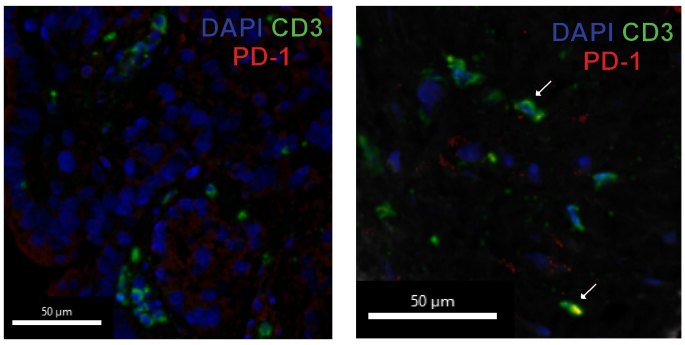

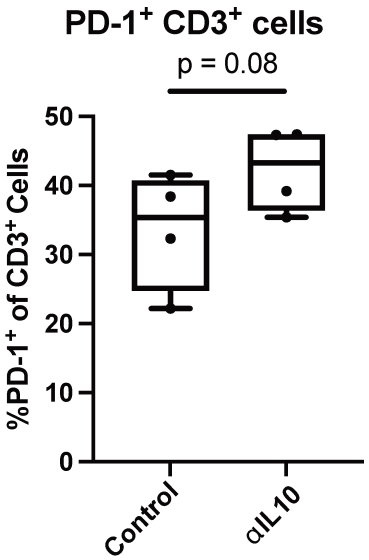

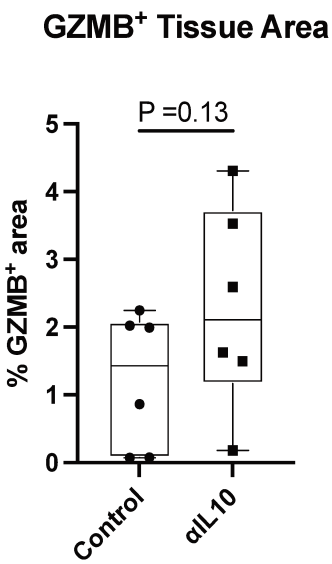

S3

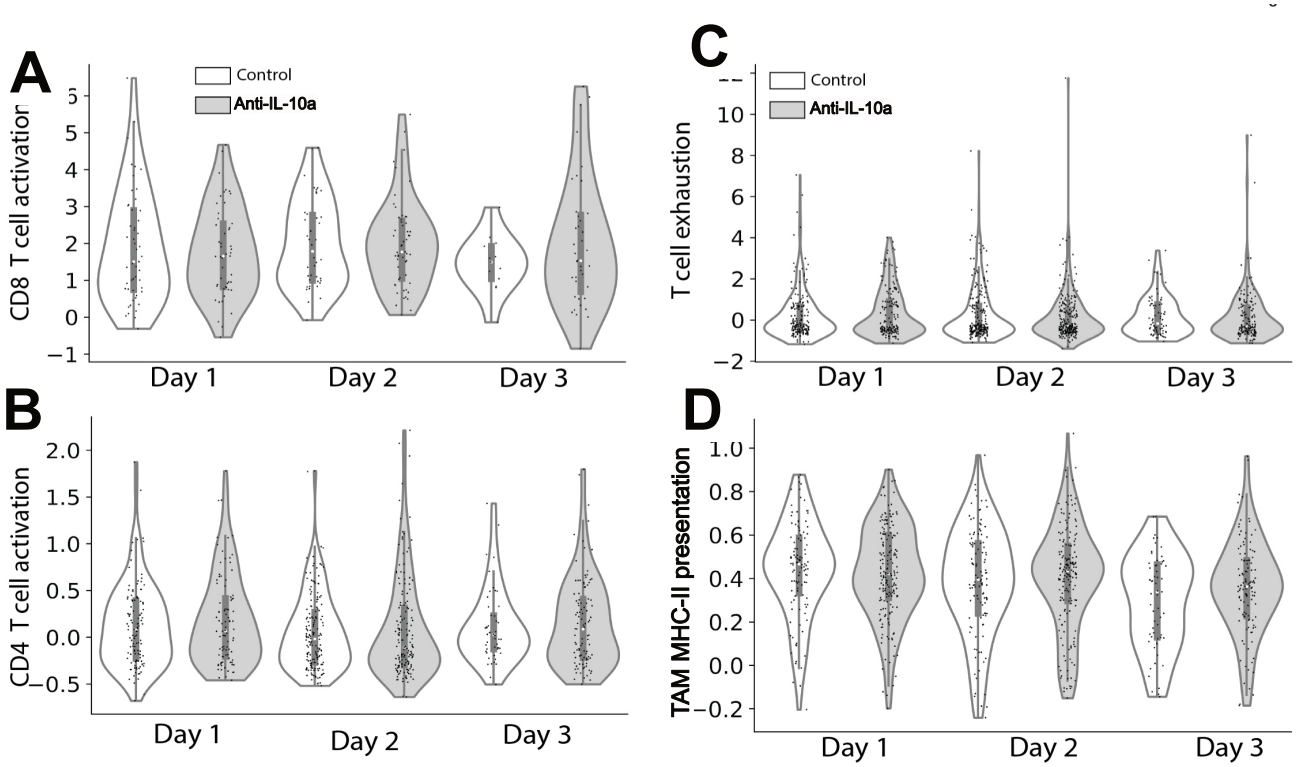
A
Control
Anti-IL-10a
CD8 T cell activation
Day 1
Day 2
Day 3
B
CD4 T cell activation
C
T cell exhaustion
D
TAM MHC-II presentation

S4

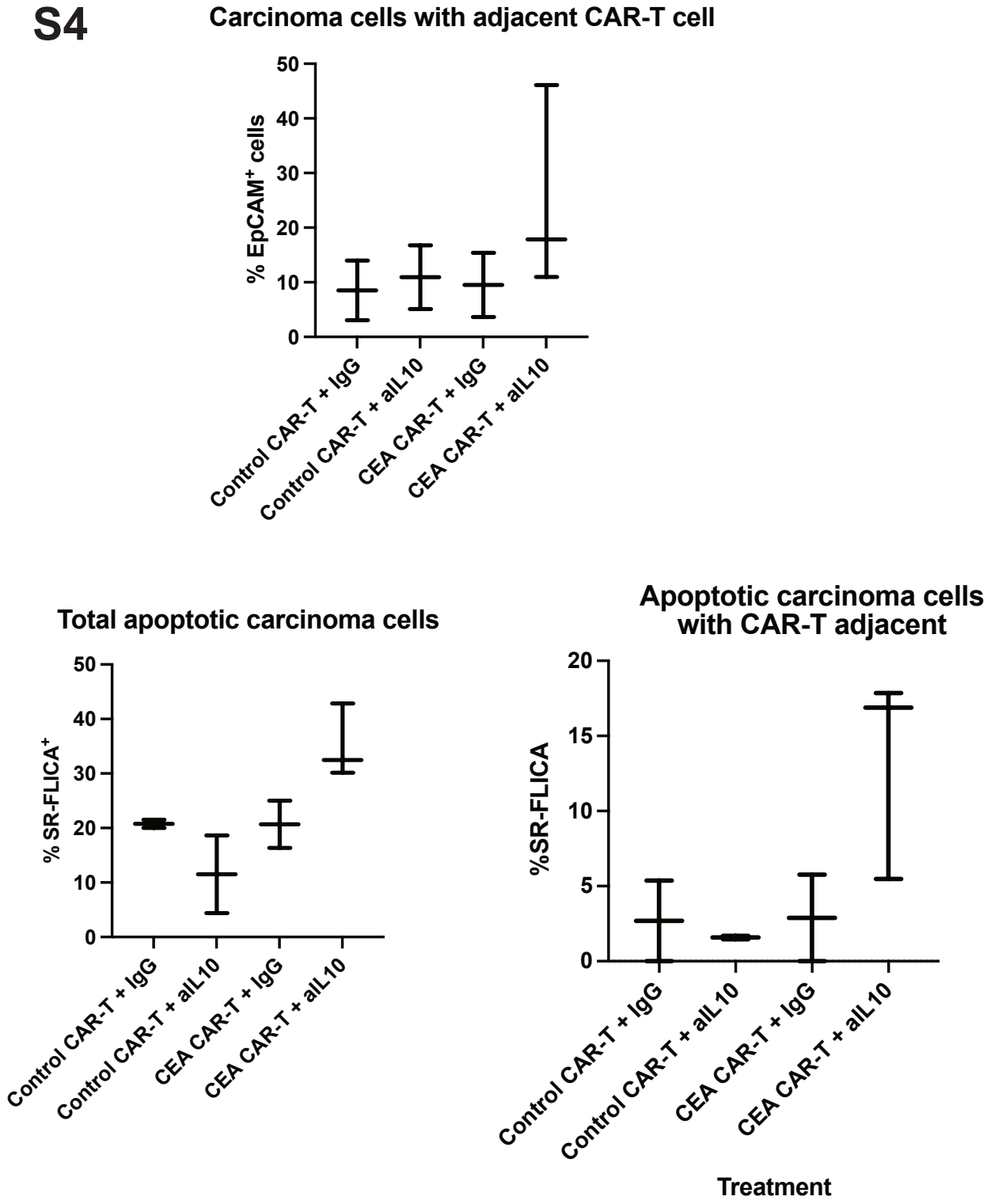
Carcinoma cells with adjacent CAR-T cell
% EpCAM+ cells
50
40
30
20
10
0
Control CAR-T + IgG
Control CAR-T + aIL10
CEA CAR-T + IgG
CEA CAR-T + aIL10
Total apoptotic carcinoma cells
% SR-FLICA+
Apoptotic carcinoma cells with CAR-T adjacent
%SR-FLICA
20
15
10
5
0
Treatment

S5

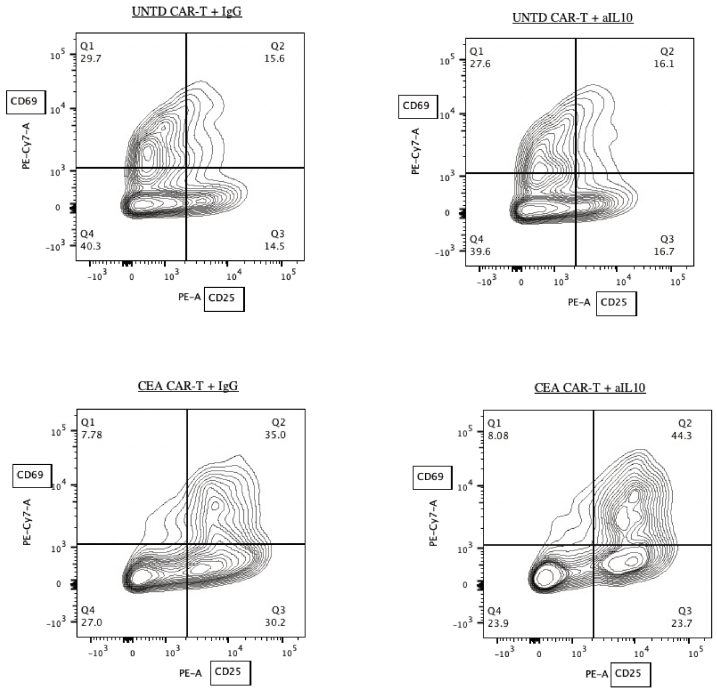
UNTD CAR-T + IgG
Q1 29.7
Q2 15.6
Q4 40.3
Q3 14.5
UNTD CAR-T + aIL10
Q1 27.6
Q2 16.1
Q4 39.6
Q3 16.7
CEA CAR-T + IgG
Q1 7.78
Q2 35.0
Q4 27.0
Q3 30.2
CEA CAR-T + aIL10
Q1 8.08
Q2 44.3
Q4 23.9
Q3 23.7
CD69
PE-Cy7-A
PE-A CD25

SUPPLEMENTARY MATERIALS:

Fig. S1.

Correlation of the highest and lowest quartiles of IL-10 expression with disease-specific survival (DSS) at 5 years in the TCGA Pan-Cancer of primary colon adenocarcinoma (COAD) dataset demonstrating improved DSS for colon cancer with low *IL10* expression ($P<0.05$), but no change in DSS for colon cancer for high vs low *PDCD1* and *HAVCR1*expression ($P>0.05$).

Fig. S2.

S2A – IL-10 cytokine was measured in TSC supernatant from n=5 tumors treated with control or αIL-10, with a marked reduction in the IL-10 detectable within the system.

S2B – Co-staining of IHC by EpCAM marking for tumor cells (red) and cleaved-Caspase-3 (CC3) for apoptotic cells (brown) indicates that the increased CC3 expression is occurring on tumor cells. $EpCAM^+$ $CC3^+$ cells are denoted with black arrows. Representative of n = 3 patient tumors.

S2C –Staining of consecutive slides of CD163 and HLA-DR. Cells positive in the same position on the consecutive slides are denoted by black arrows. Representative of n = 3 patient tumors.

S2D - Multiplex IHC was performed for T cells (CD3, green), PD-1 (red), and nuclei (DAPI, blue). Quantification of proportion of $PD\text{-}1^+$ $CD3^+$ cells are also shown (n = 6 patient tumors). Granzyme B^+ by tissue area similarly stained by IHC and quantified. Scale bar = 50 µm. Data points represent each human tumor sample. Student's t test.

Fig. S3.

Two separate patient tumors were collected on sequential days 1, 2, and 3 of treatment with IL-10 blocking antibody or control antibody. Single cell RNA sequencing was performed on all samples. Violin plots of gene expression of cytolytic and activation gene signatures in the in $CD8^+$ and $CD4^+$ T cell subsets as well as TAM subset. The activation gene signature consists of *CD69*, *FASLG*, *CD27*, *CD28*, *TNFRSF9*, *TNFRSF4*, *LAMP1*, *EOMES*, *TBX21*(A-B). The exhausted gene signature consists of *PDCD1, CTLA4, HAVCR2, TIGIT*, and *LAG3* (C). Last, violin plot of the MHC-II presentation genes in the Reactome pathway in the macrophage cell cluster (D).

Fig. S4.

Results of low dose (10^5 rather than 10^6) CAR-T cell showing similarly increased CAR-T cell migration and CAR-T cell mediated carcinoma cell apoptosis which did not meet statistical significance.

Fig. S5.

Representative flow cytometry plot and quantification of cells gated for $CFSE^+$ T cells which are also positive for CD25 and/or CD69 from experiments depicted in Fig. 6C.

Sullivan KM, *et al. Gut* 2022;0:1–13. doi: 10.1136/gutjnl-2021-325808

Supplemental Materials and Methods

Tumor slice culture

Slice culture of freshly resected human CRLM tumors was performed as previously described [35 36 40]. Briefly, sterile cores from tumor specimens were obtained using a 6 mm punch biopsy in the operating room immediately following resection, under the review of the on-call surgical pathologist to ensure the retention of adequate tissue for diagnosis and margin assessment. The cores were placed in Belzer UW Cold Storage solution on ice. Using a vibratome (Leica Biosystems), 250 µm slices were cut sequentially and placed on a permeable PTFE membrane with 0.4 µm pores (Millicell, MilliporeSigma, Burlington, MA), placed in a 24-well dish containing RPMI media with 10% fetal bovine serum (FBS) and 1% penicillin/streptomycin but without any additional immune-activating factors or cytokines. Slice cultures were incubated overnight at 37°C and then treated with 10% FBS RPMI media containing either 20 µg/mL of IgG isotype control (#553447, BD Biosciences), 20 µg/mL of αPD-11 (#562138, Biolegend), or 20 µg/mL of αIL-10 (#501407, Biolegend) For an individual tumor sample, slices were distributed evenly and randomly from throughout the tumor with 3 slices per treatment group to account for confounding from intra-tumor heterogeneity. Slices were only excluded for technical failure of slicing and no treated slices were excluded. Treatment samples were not blinded when analyzing results. The dose of αIL-10 was chosen based upon a dose titration experiment using 5, 10, and 20 µg/ml concentrations of antibody, showing a maximal effect at 20 µg/ml. Additional experiments used 20 µg/mL of anti-MHC class I (purified mouse anti-human HLA-ABC #555551, BD Biosciences) and/or 20 µg/mL of anti-MHC class II (purified mouse anti-human HLA-DR, DP, DQ #555557, BD Biosciences). If the slices were to be maintained in culture for more than 3 days, half the volume of media was changed with fresh treatment after 72 hours.

In situ hybridization (ISH) and multicolor immunohistochemistry (mIHC)

For ISH, FFPE tissues were sectioned at 4 µm onto positively-charged slides and baked for 1 hour at 60°C. The slides were then dewaxed and stained on a Leica BOND Rx Stainer (Leica, Buffalo Grove, IL) using Leica Bond reagents for dewaxing (Dewax Solution), antigen retrieval with Epitope Retrieval Solution 2 for 15 minutes at 95°C, cell permeabilization with 0.5% Triton-X in PBS for 30 minutes at RT and rinsing after each step (Bond Wash Solution). All steps after epitope retrieval were performed at RT. The slides were then blocked with hydrogen peroxide for 10 minutes and incubated with the ACD target probe, IFN-g (#550478-C3, Advanced Cell Diagnostics) or IL10Ra (#498058, Advanced Cell Diagnostics) and IL10 (#602058-C2, Advanced Cell Diagnostics), at 42°C for 120 minutes. After the probe incubation, the staining proceeded with the ACD RNAscope LS Multiplex Fluorescent Reagent Kit (#322800) for the amplification and detection steps, followed by Opal fluor (Opal 650 for IFN-g, Opal 570/650 for IL10RA/IL10) at 1:750 for 10 minutes. Slides were removed from the Stainer and stained with DAPI for 5 minutes, rinsed for 5 minutes, and a coverslip was mounted with Prolong Gold Antifade reagent (Invitrogen/Life Technologies, Grand Island, NY). Slides were imaged with Leica SP8 confocal microscope.

For the mIHC staining, the coverslip of slides was removed in deionized water and stained on a Leica BOND Rx using Leica Bond reagents for dewaxing (Dewax Solution), antibody stripping (Epitope Retrieval Solution 2), and rinsing after each step (Bond Wash Solution). Antibody stripping steps were performed at 100°C with all other steps at ambient temperature. Endogenous peroxidase was blocked with 3% H_2O_2 for 5 minutes followed by protein blocking with TCT buffer (0.05M Tris, 0.15M NaCl, 0.25% Casein, 0.1% Tween 20, 0.05% ProClin300 pH 7.6) for 10 minutes. The first

primary antibody (position 1) was applied for 60 minutes followed by the secondary antibody application for 10 minutes and the application of the tertiary TSA-amplification reagent (PerkinElmer OPAL fluor) for 10 minutes. The primary antibodies used were EpCAM (Opal 690, 32402, Biolegend) in position 1, HLA-DR (Opal 620, M0746, Dako) in position 2, CD3 (Opal 570, RM9107, ThermoFisher) in position 3, and CD163/68 (Opal 540, BSB3276, BioSB and M0876, Dako) in position 4 followed by the Powervision Mouse-HRP secondary antibody (Leica). A high stringency wash was performed after the secondary and tertiary applications using high-salt TBST solution (0.05M Tris, 0.3M NaCl, and 0.1% Tween-20, pH 7.2-7.6). Polymer HRP was used for all secondary applications, as specified in the table. The primary and secondary antibodies were stripped with retrieval solution for 20 minutes before repeating the process with the second primary antibody (position 2) starting with a new application of 3% H_2O_2. The process was repeated until all positions were completed; however, there was no stripping step after the final position. Slides were removed from the stainer and stained with DAPI for 5 minutes, rinsed for 5 minutes, and coverslip mounted with Prolong Gold Antifade reagent (Invitrogen/Life Technologies, Grand Island, NY). Slides were imaged with Leica SP8 confocal microscope.

For combination of mIHC and ISH mIHC staining was done either before or after ISH. Slides were imaged after each step. ISH labeling was bleached when mIHC was performed subsequently. To combine the signals from ISH and mIHC, images were overlaid, and areas of perfect nuclear overlap were analyzed. Images were analyzed using Imaris (Bitplane). Parameters for each segmented cell including area, sphericity, mean intensity values were exported as comma separated value (CSV) files. Mean intensity values were normalized via z-score normalization. CSV files were analyzed via Flowjo (Beckton Dickinson).

Reverse phase protein array (RPPA)

Protein microarrays were printed and processed as described previously [41 42]. Briefly, tumor slices were lysed in 2% SDS lysis buffers as described previously[41 42]. Tumor slice lysates were printed onto 16-pad nitrocellulose coated slides (Grace Biolabs, OR, US) using Aushon 2470 microarrayer (Aushon BioSystems, MA, US). Each sample was printed in duplicate, and slides were stored at – 20°C until processing. Slides were then washed 2-3 times with PBS for 5 min each and blocked with Odyssey Blocking Buffer (OBB, Licor, NE, USA) for one hour at room temperature. After blocking, arrays were incubated with primary antibodies in OBB at 4°C overnight. The next day, arrays were washed thrice with PBS and incubated with IRDye labeled secondary antibodies in OBB for 1 hour at room temperature. Following incubation, slides were scanned using Licor Odyssey CLX Scanner (LiCOR). Total signal intensity from each spot was quantified using Array-Pro analyzer software package (Media Cybernetics, MD, USA). The measurement of a specific protein from an individual sample was normalized to total beta-actin (Sigma, Cat #A1978).

Immunohistochemistry (IHC)

At the desired times following treatment, slices were removed from culture and fixed in 10% formalin. Tissue was then paraffin embedded and 4 µm thick tissue slices were mounted on slides for storage. Slides were de-paraffinized in xylene and rehydrated through graded ethanol followed by heat mediated antigen retrieval using 10 mM Sodium Citrate Buffer (pH 6.0) and blocked with 3% hydrogen peroxide for 5 minutes and Background Buster (Innovex Biosciences) for 30 minutes. IHC was performed via incubations with one primary antibody at 4°C overnight followed by host-matched secondary polymer reagent and color substrate. Primary antibodies used were as follows: CD8 (M7103, Dako), HLA-DR

(M0746, Dako), CD163 (ab189915, Abcam), and cleaved-Caspase-3 (#9661, Cell Signal Technologies). Secondary reagents were ImmPress Rabbit HRP and Mouse HRP (Vector Laboratories). Color development was performed using DAB Quanto (Brown HRP; Fisher Scientific). Slides were counterstained with Harris hematoxylin (Sigma) as appropriate, dehydrated, and mounted. The transversely cut slides were imaged over multiple 20x hpf to visualize the entire thickness of the slice.

For dual-color IHC staining, sections were first stained as above with a primary antibody against cleaved-Caspase-3 (#9661, Cell Signal Technologies) and host-match secondary antibody Immpress Rabbit HRP (Vector Laboratories). Color development was performed using DAB Quanto (Brown HRP; Fisher Scientific). Slides were washed with TBST and PBS washing buffers, re-blocked with Background Buster for 15 minutes, and re-incubated with EpCAM (ab124825, Abcam) as the primary antibody. Immpress alkaline phosphatase (AP) anti-rabbit polymer (Vector Laboratories) was then used as secondary antibody and color development was performed with Warp Red substrate (WR 806CHC, Biocare). Slides were washed with TBST and PBS and counterstained with Harris hematoxylin (Sigma) and directly mounted with Aqua-mount (13800, Lerner Laboratories).

Stained tissue sections were digitally scanned and uploaded to NanoZoomer Digital Pathology (Hamamatsu) image viewing software. Images we exported and positive DAB cells and hematoxylin-stained nuclei were visually counted using Fiji ImageJ software. Each data point represents one case consisting of multiple (at least 2) slices and a minimum of 2 hpf within a single slice to account for both intra- and inter-tumoral heterogeneity.

Mice, liver metastasis (LM) in vivo model and myeloid cell isolation

C57BL/6 male mice (6–8-week-old) obtained from Jackson Laboratories were bred and maintained under pathogen free conditions at Roger Williams Medical Center (RWMC) animal facility. All surgical procedures were approved by RWMC Institutional Animal Care and Use Committee (IACUC). To generate LM, mice were anesthetized and injected with $2.5x10^6$ MC38CEA (generous gift from Dr. Jeffrey Schlom) via spleen followed by splenectomy to confine metastases to the liver. Liver non-parenchymal cells were isolated from LM, four days post-tumor generation, as previously described[15]. Immunomagnetic beads against CD11b were used to purify bulk hepatic MDSCs (Miltenyi Biotech). Typical purity of beaded $CD11b^+$ cells were 80–90% from mice with LM.

CAR-T generation, proliferation assay and cytotoxicity assay

CAR-T cells were generated from mouse splenocytes as described previously[43] and MC38CEA cells were used as target tumor cells. Isolated myeloid cells were isolated from LM tumor bearing mice livers. CAR-T cells were carboxyfluorescein diacetate succinimidyl ester (CFSE, Life Technologies) labeled as per company's protocol. MC38CEA cells were plated at $2x10^4$ cells/well in 96-well cell culture plate (BD Bioscience) with myeloid cells + CAR-T cells in a 1:1:1 ratio. Cells were treated with 100ng/ml or 200 ng/ml and 400 ng/ml of IL-10 antibody (JES5-2A5, Biolegend). After 24 hours, cells were removed and analyzed for CFSE using flow cytometry. Supernatant was collected and analyzed for LDH as per manufacturer's protocol (Promega). No exclusion of data points was necessary and treatment groups were not able to be blinded during analysis. N = 3 biological replicates and n = 4 technical replicates were performed.

Flow cytometry

Antibodies specific for the following markers were used: CD3 (17A2, BD Bioscience), IL-10 (JES5-16E3, BD Bioscience), IL-10R (1B1.3a, Biolegend), CD11b (M1/70, BD Bioscience), Gr1 (RB6-8C5, Biolegend), and anti-idiotypic CEA-Fc (Sorrento Therapeutics). For human CAR-T cells, cells were stained for CFSE, CD25 (BD Bioscience, 560989) and CD69 (Invitrogen, 25069941). For intracellular staining, the BD Bioscience Fixation/Permeabilization kit was used. Unstained and isotype controls were used for gating purposes. Cells were collected for analysis using Cytoflex LX (Beckman Coulter) and post-acquisition analysis was performed using FlowJo software (BD Bioscience).

Live imaging

CRLM tumor slices cultures were created as described above. Untransduced control or CAR-T cells were thawed, washed, and stained with CFSE at a concentration of 0.5 mM. One million of the stained control or antigen-specific CAR-T cells were added on top of slices to be treated in culture followed by either control or αIL-10 to the supernatant added to the media, and slices with CAR-T cells and antibody treatment were incubated for 1 day. Treatment 10^5 CAR-T cell resulted in similar but non-significant results compared to 10^6 (Fig. S4). The treated CRLM tumor slices were transferred into fresh media in a 48 well plate with 10 mg/mL Alexa 647 EpCAM antibody to stain tumor cells (Biolegend, San Diego, CA) and SR-FLICA reagent to stain apoptotic cells per the manufacturer's instructions (ImmunoChemistry Technologies, Bloomington, MN) and were incubated for 3 hours at 37°C for staining. The slices were then stained for nuclei using 10 mg/mL Hoechst 33342 (ImmunoChemistry Technologies) for 10 min. The slices were washed twice with PBS and returned with their original media containing the CAR-T cell and antibody treatment to an 8-well culture slide (Ibidi USA, Fitchburg, WI) for imaging. Tissue culture conditions were maintained as close to cell culture incubator as possible while imaging was performed, by using a heated covered stage (PeCon,

Erbach, Germany) to 37°C while flushing warmed, humidified CO_2 through the enclosure. The slices were imaged using a Leica SP8X confocal microscope (Leica Microsystems, Wetzlar, Germany) at 20x magnification. For each treated slice, images were collected for 1 hour at three different positions throughout the slice with a z-stack of 20 μm. One slice was used per treatment group per patient given imaging constraints with random sequential slices assigned to each treatment group.

In an experiment blocking the IL-10R on CAR-T, the CAR-T were thawed and incubated overnight in tissue culture media with 20 mg/mL of either control or αIL-10R. The CAR-T cells were washed with PBS, spun, and resuspended in media. They were stained with CFSE and placed directly into the CRLM tissue slice culture media without additional treatment or antibody blockade. After 1 day, slices were stained and imaged as above.

No slices or data were excluded from analysis. Treatment groups were unable to be blinded for imaging or analysis. Image processing and data analysis were performed on Leica LAS X software (Leica Microsystems, Wetzlar, Germany) and Imaris software (Bitplane USA, Concord, MA). The data and images obtained were visualized using a maximum intensity projection of the 20 μm z-stack. The $EpCAM^+$, $CFSE^+$, $SR\text{-}FLICA^+$ cells were counted manually. All cells observed throughout the time imaged at each position in each slice were counted.

Bulk RNA sequencing

CRLM slice culture treated with either untransduced or anti-CEA CAR-T cells either with or without IL-10 blocking antibody as described above. RNA was extracted from slices using Qiagen RNEasy kit

per the manufacturer's instructions. Samples were submitted to the Northwest Genomics Center for NGS sequencing.

Single cell RNA sequencing (scRNAseq)

Tumor slice dissociation

Tumor slices were dissociated using the MACS Tumor Dissociation Kit (MiltenyiBiotec, Auburn, CA) according to the manufacturer's "dissociation of soft tumors" protocol. Prior to dissociation, an enzyme mix was prepared by adding fresh aliquots of enzymes A, R and H with the recommended volumes to RPMI 1640 medium in a sterile "gentleMACS C" tube. The initial mechanical dissociation step was performed by running the "h_tumor_01 program." Slices were then incubated at 37°C for 20-30 minutes under continuous rotation using the MACSmix Tube Rotator followed by a second mechanical dissociation step, "h_tumor_02 program". Slices were then visually evaluated and tubes were incubated for an additional 20 minutes at 37◦ C if undissociated tissue was visible. Slice tissue was further dissociated by running the "h_tumor_03" program. After a short spin, the cell suspension was passed through a 70 µm MACS SmartStrainer. The strainer was washed with a solution of 0.04% (w/v) molecular biology grade BSA (Gemini Bio Products) in PBS. Finally, the cell suspension was strained through a 30 µm MACS SmartStrainer. Cells were spun down at 300×g and supernatant was removed.

Removal of dead cells from single cell suspension

Dead cells were removed from single cell suspensions with the Dead Cell Removal kit (MiltenyiBiotec) and according to the Dead Cell Removal Rev B protocol (10X Genomics, Pleasanton, CA). Cells were resuspended in Dead Cell Removal MicroBeads and incubated for 15 minutes at room temperature. Meanwhile, an MS column (MiltenyiBiotec) was rinsed with binding buffer. The cell suspension was then diluted and applied to the MS column on a MiniMACS separator. The effluent containing the live

single cells in binding buffer was collected into sterile tubes. The binding buffer was then replaced with PBS containing 0.04% BSA through two wash steps. Wide-bore pipette tips (Rainin, Columbus, OH) were used to ensure minimum damage to single cells.

Single cell suspension preparation for 10X Genomics Single Cell experiments

The cell suspension was mixed with Trypan Blue, quantified with a Countess Automated Cell Counter (Life Technologies, Waltham, MA), and confirmed with a hemocytometer. Based on the cell concentration and the targeted cell recovery, the corresponding volume of cell suspension was mixed with nuclease free water and loaded on the Chromium Controller according to the Chromium Single Cell 3' Reagent Kits v2 protocol (10X Genomics). On average, 17,000 cells in 33.8 µl were loaded into each Chromium droplet generation microfluidic device to target the maximum cell recovery number of 10,000.

10X Droplet Sequencing

Cellular suspensions were loaded on a Chromium instrument (10X Genomics, San Francisco, CA) to generate single-cell Gelbead-In-EMulsion (GEM) droplets. Reverse transcription (RT) was performed in a C1000 Touch thermocycler (Biorad, Hercules, CA). After RT, GEMs were harvested and the cDNAs were amplified and cleaned with SPRIselect Reagent Kit (Beckman Coulter, Brea, CA). Indexed sequencing libraries were constructed using the Chromium Single-Cell 3' Library Kit (version 2) for enzymatic fragmentation, end-repair, A-tailing, adapter ligation, ligation cleanup, sample index PCR, and PCR cleanup. The barcoded sequencing libraries were quantified by quantitative PCR using the KAPA Library Quantification Kit (KAPA Biosystems, Wilmington, MA). Sequencing libraries were loaded on a NextSeq500 (Illumina, San Diego, CA) and run 150 cycles (26 bp for Read 1 and 124 bp for Read 2). Two indexed (multiplexed) libraries (i.e. Control, anti-IL-10) were loaded on to one flowcell to obtain a sequencing depth of approximately 100,000 reads per cell. Reads were aligned to

the human genome (GRCh38) and quantified using the Cell Ranger (version 2.0, http://cf.10xgenomics.com/releases/cell-exp/ cellranger-2.0.0.tar.gz). Poor-quality cells/GEMs, defined as those expressing a high proportion (>10%) of mitochondrial genes or a low number of total genes (<200) were discarded. Unique transcripts were identified by 10X unique molecular indexes (UMIs). UMI counts were normalized by adjusting for library size and dividing by the median count of each cell, as implemented by the Cell Ranger R kit (version 2.0, http://cf.10xgenomics.com/supp/cell-exp/¬rkit-install-2.0.0.R).

Cell type classification and clustering

Sample UMI data were aggregated and the gene-cell matrix was normalized to give each gene a mean of 0 and standard deviation of 1. Principal Component Analysis was performed, and the top 30 components used to calculate a Uniform Manifold Approximation and Projection (UMAP) for visualization of all single cells in a two-dimensional space. Cells were clustered by the Leiden algorithm (26) as implemented with the SCANPY toolkit (27).

Table S1 – treatment antibodies

Antibody	**Manufacturer**	**Catalog no.**
Monoclonal IgG	BD Biosciences	#553447
Anti-IL-10	Biolegend	#501407
Anti-PD-1	BD Biosciences	#562138
Anti-MHC I	BD Biosciences	#555551
Anti-MHC II	BD Biosciences	#555557

Table S2 – ISH probes, mIHC antibodies, and live fluorescent imaging antibodies**Antibody**	**Fluorophore**	**Manufacturer**	**Catalog no.**
IFNG	Opal 650	Advanced Cell Diagnostics	#550478-C3
IL10RA	Opal 570	Advanced Cell Diagnostics	#498058
IL10	Opal 650	Advanced Cell Diagnostics	#602058-C2
EpCAM	Opal 690	Biolegend	32402
HLA-DR	Opal 620	Dako	M0746
CD3	Opal 570	ThermoFisher	RM9107
CD163	Opal 540	BioSB	BSB3276
CD68	Opal 540	Dako	M0876
EpCAM	Alexa 647	Biolegend	324212
Poly caspases	SR-FLICA	ImmunoChemistry Technologies	916

Table S3 – IHC antibodies

Antibody	**Manufacturer**	**Catalog no.**
cleaved-Caspase-3	Cell Signal Technologies	#9661
CD163	Abcam	ab189915
HLA-DR	Dako	M0746
CD4	Dako	M7310
CD8	Dako	M7103

Table S4 – flow cytometry antibodies

Antibody	**Manufacturer**	**Catalog no.**
CD3	BD Bioscience	17A2
IL-10	BD Bioscience	JES5-16E3
IL-10R	Biolegend	1B1.3a
CD11b	BD Bioscience	M1/70
Gr1	Biolegend	RB6-8C5
anti-idiotypic CEA-Fc	Sorrento Therapeutics	
CD69	Invitrogen	25069941
CD25	BD Bioscience	560989

S1

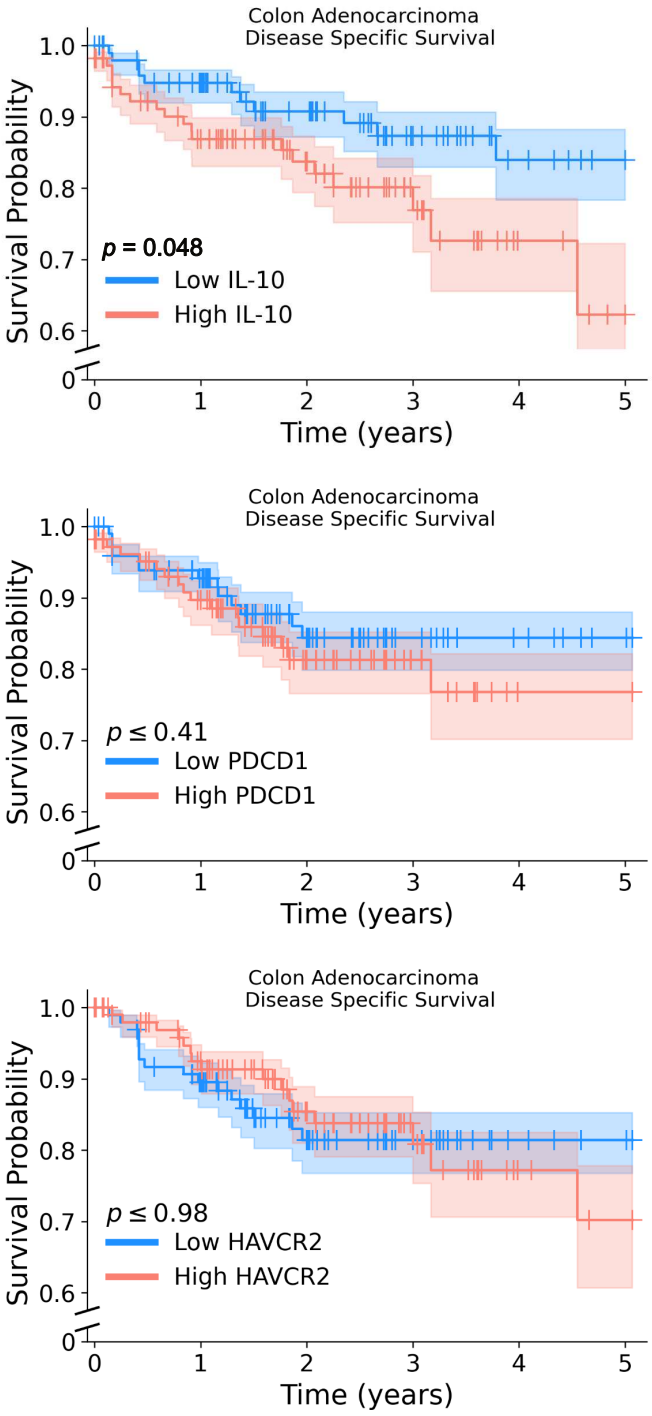
Colon Adenocarcinoma
Disease Specific Survival
Survival Probability
1.0
0.9
0.8
0.7
0.6
0
p = 0.048
Low IL-10
High IL-10
0
1
2
3
4
5
Time (years)
Colon Adenocarcinoma
Disease Specific Survival
Survival Probability
p ≤ 0.41
Low PDCD1
High PDCD1
Time (years)
Colon Adenocarcinoma
Disease Specific Survival
Survival Probability
p ≤ 0.98
Low HAVCR2
High HAVCR2
Time (years)

S2A

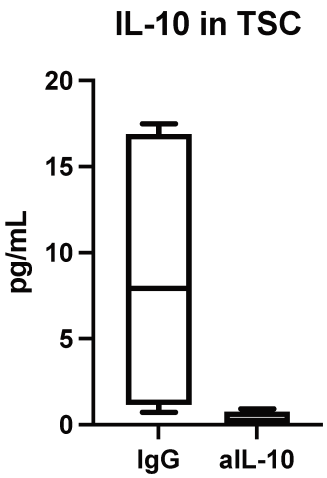

S2B

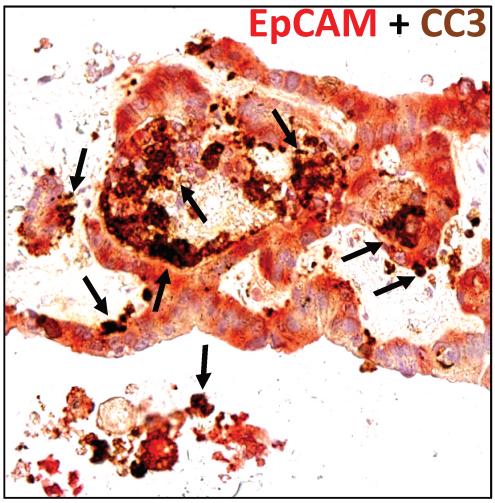

S2C

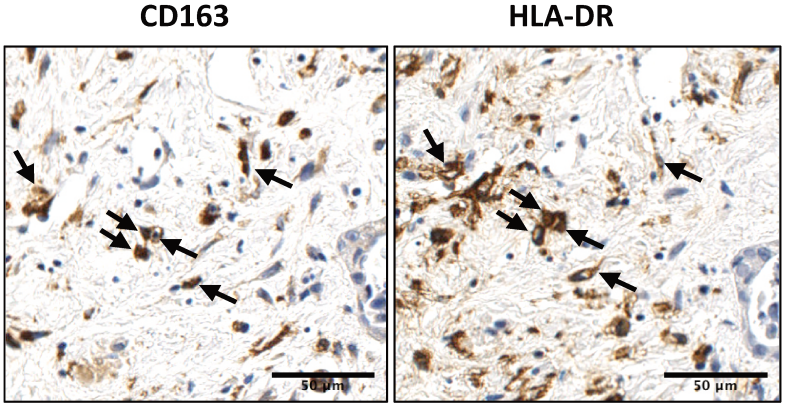

S2D

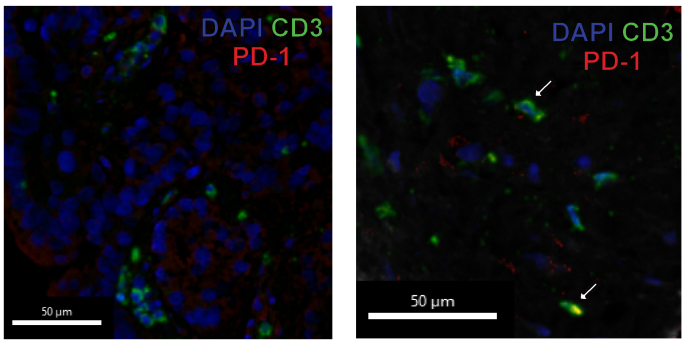

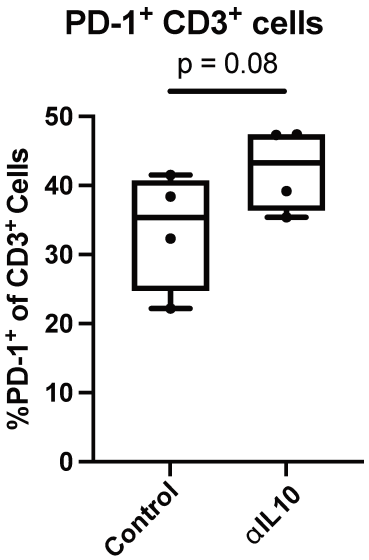

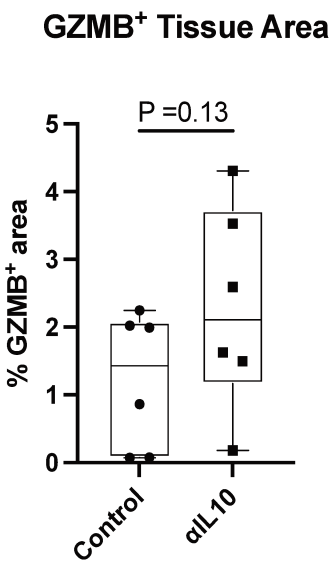

S3

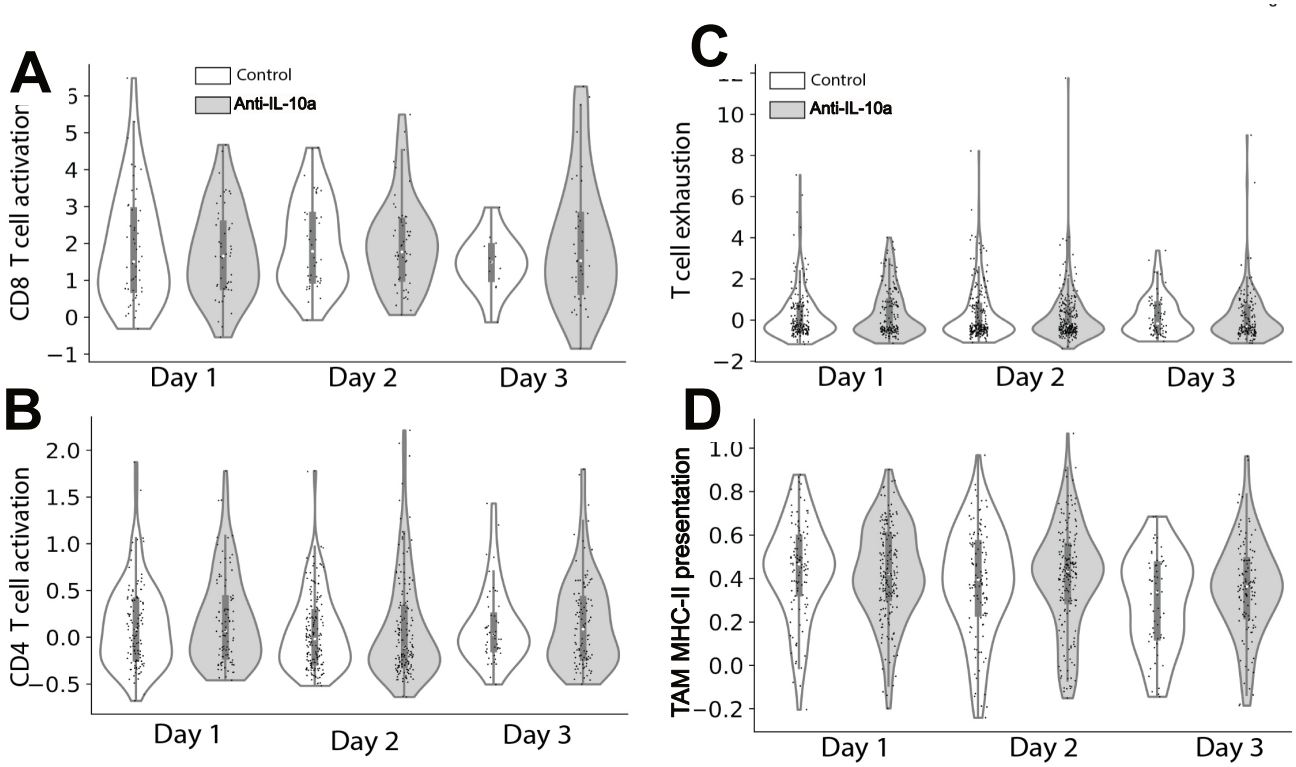
A
Control
Anti-IL-10a
CD8 T cell activation
Day 1
Day 2
Day 3
B
CD4 T cell activation
C
T cell exhaustion
D
TAM MHC-II presentation

S4

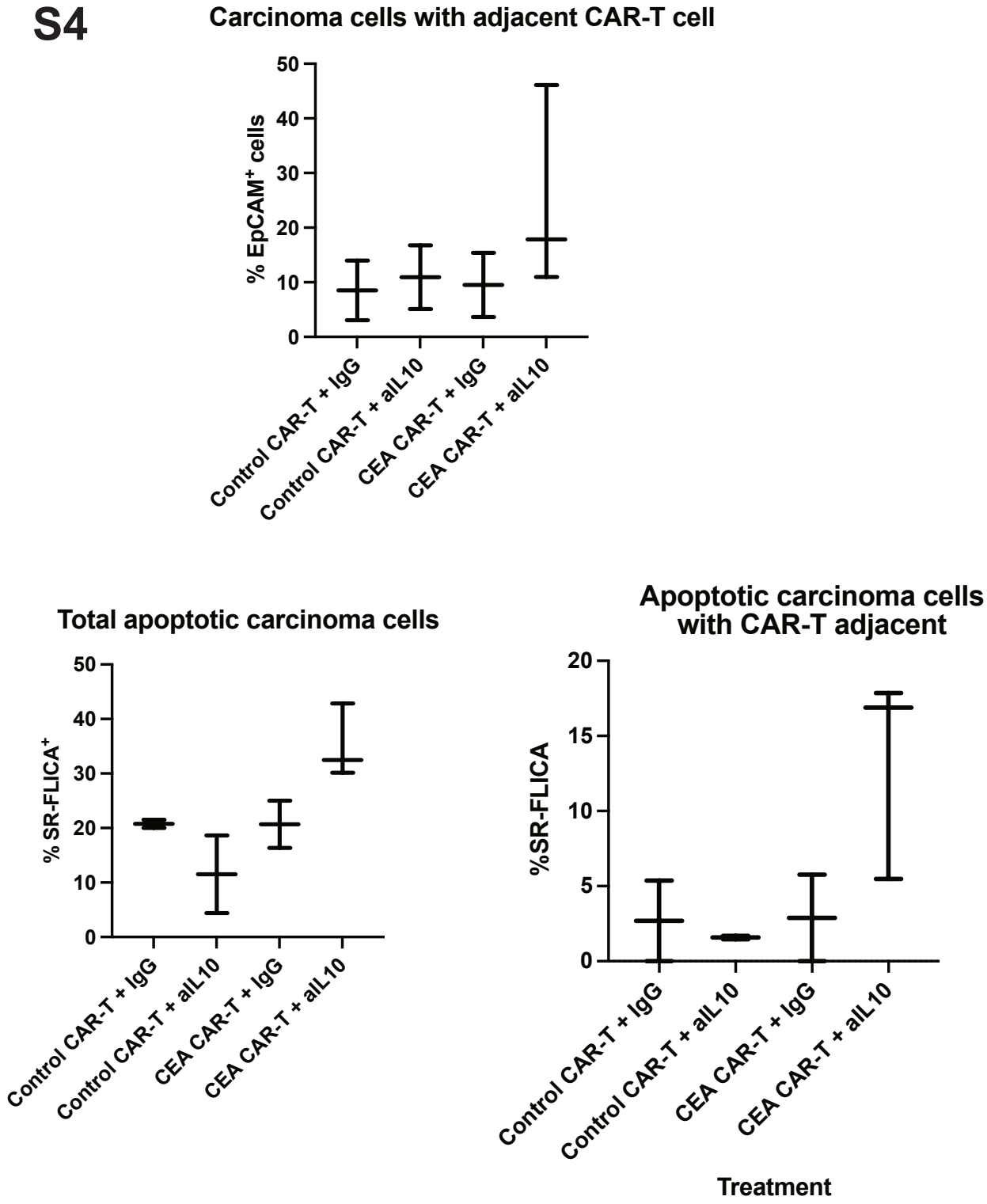
Carcinoma cells with adjacent CAR-T cell
% EpCAM+ cells
50
40
30
20
10
0
Control CAR-T + IgG
Control CAR-T + aIL10
CEA CAR-T + IgG
CEA CAR-T + aIL10
Total apoptotic carcinoma cells
% SR-FLICA+
Apoptotic carcinoma cells with CAR-T adjacent
%SR-FLICA
20
15
10
5
0
Treatment

S5

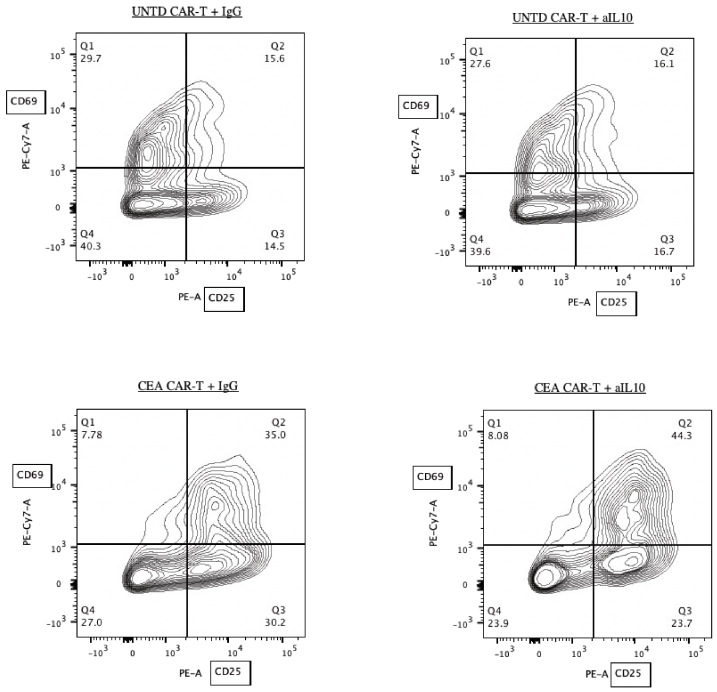
UNTD CAR-T + IgG
Q1 29.7
Q2 15.6
Q4 40.3
Q3 14.5
UNTD CAR-T + aIL10
Q1 27.6
Q2 16.1
Q4 39.6
Q3 16.7
CEA CAR-T + IgG
Q1 7.78
Q2 35.0
Q4 27.0
Q3 30.2
CEA CAR-T + aIL10
Q1 8.08
Q2 44.3
Q4 23.9
Q3 23.7
CD69
PE-Cy7-A
PE-A CD25